ISSN 1849–0751 (On–line)
ISSN 0013–7448 (Print)
UDK 621.31

https://doi.org/10.37798/EN2023724

Journal of Energy

VOLUME 72 Number 4 | 2023

ENERGIJA 72

03 Susanta K. Das, Jinsu Kim
Power Management Strategy of a PEM Fuel Cell-Battery Powered Electric Vehicle

09 Karlo Petrović, Antonio Petošić, Tomislav Župan
Application of Adaptive Finite Focus Beamforming Method for Localization of Low-frequency Transformer Sound

15 Ferdinand Fuhrmann, Anna Maly, Martin Blass, Jakub Waikat, Fredi Belavic, Franz Graf
3D Acoustic Heat-Maps for Transformer Monitoring Applications

19 Martin Siegel, Christoph Kattmann, Chandra Prakash Beura, Michael Beltle, Stefan Tenbohlen
Partial Discharge Monitoring of Power Transformers by Calibrated UHF Measurements

28 L. Luttenberger Marić, D. Borić, H. Keko, J. Aranda, M. Kirinčić
Local Aggregator Enhanced Possibilities Coupling Energy Savings and Demand Response Activations

Journal of Energy

Scientific Professional Journal Of Energy, Electricity, Power Systems
Online ISSN 1849–0751, Print ISSN 0013–7448, VOL 72
https://doi.org/10.37798/EN2023724

Published by
HEP d.d., Ulica grada Vukovara 37, HR–10000 Zagreb
HRO CIGRÉ, Berislavićeva 6, HR–10000 Zagreb

EDITORIAL

The first paper is “Power Management Strategy of a PEM Fuel Cell-Battery Powered Electric Vehicle”. In this study, a MATLAB-Simulink-based mathematical simulation model for a proton exchange membrane (PEM) fuel cell and battery-powered electric vehicle was developed. The model takes into account real commercial driving cycles and vehicle dynamics and aims to accurately estimate the total onboard power requirements. The fuel cell serves as the primary power source, while the battery serves as an additional source for power peaks. The simulation, which was optimized for battery state-of-charge, drive torque and vehicle performance, has shown that the power requirement of the electric vehicle is significantly influenced by the interaction of fuel cell and battery management systems as well as driver behavior. The study provides valuable insights into the power management mechanisms of fuel cell and battery-powered electric vehicles and offers clues for further investigation and research in this field.

The second paper is entitled “Application of Adaptive Finite Focus Beamforming Method for Localization of Low-frequency Transformer Sound”. In this paper, an adaptive linearly constrained finite focus beamforming method with minimum variance is presented to improve the accuracy and resolution of the localization of low-frequency transformer noise sources. The study includes simulations on virtual arrays to determine the array size and compare the effects of different beamforming algorithms on the accuracy and resolution of sound localization. The developed algorithm is evaluated against infinite and finite beamforming for localization of overall noise and noise at specific harmonics. The study shows that the adaptive finite focus beamforming method increases the spatial resolution and localization accuracy for low-frequency noise and meets the specific requirements of transformer noise localization.

The third paper is “3D Acoustic Heat-Maps for Transformer Monitoring Applications”. This paper presents an innovative approach to measure and visualize acoustic emissions from transformers to improve monitoring for anomaly detection and predictive maintenance. The proposed method introduces 3D acoustic heatmaps to visualize acoustic emission patterns over the surface of the transformer. By combining a 3D point cloud, a microphone array and beamforming algorithms, the authors generate a distributed representation of acoustic emissions. This novel method uses acoustic sensor data to create 3D acoustic heatmaps, which provide a powerful tool for transformer testing and modeling. The integration of a microphone array with a 3D model enables a comprehensive approach. These models are used to automatically predict anomalies and potential failure events by analyzing the acoustic radiation patterns of the transformer.

The fourth article is entitled “Partial Discharge Monitoring of Power Transformers by Calibrated UHF Measurements”. The paper deals with partial discharge (PD) measurement as an established technique for detecting local defects in the oil/paper insulation of transformers. The electromagnetic emissions of the PD are detected with a UHF sensor that is inserted into the transformer tank. The importance of PD measurement is emphasized in the standard for charge-based electrical measurements. To ensure comparability between different UHF systems and sensors, a standardized calibration procedure is essential. The paper presents a calibrated PD monitoring system based on the recently described calibration process in Cigré TB 861 and two types of UHF PD sensors for power transformers. In addition, case studies of various power transformers equipped with UHF sensors and monitoring systems are presented, demonstrating the benefits of UHF technology for on-site acceptance testing, continuous monitoring and diagnostic purposes.

The last paper is “Local Aggregator Enhanced Possibilities Coupling Energy Savings and Demand Response Activations”. The paper addresses the role of energy communities and local flexibility aggregators in decentralized and decarbonized energy systems and identifies challenges in the technical and regulatory framework. It emphasizes the need for clear communication and user-friendly engagement to balance long-term energy savings and short-term flexibility activations. The discussion outlines potential conflicts in optimization goals and highlights the importance of accessible applications for consumer engagement, favoring semantic data integration over increased sampling frequency. The paper argues for sustainable business models with consistent monitoring of energy savings, focusing on user-friendly applications for program monitoring. Finally, insights into user-centric approaches to sustainable energy communities are provided, emphasizing the integration of long-term energy savings.

Igor Kuzle
Editor–in–Chief

Journal of Energy

VOLUME 72 Number 4 | 2023

journal homepage: http://journalofenergy.com/

Power Management Strategy of a PEM Fuel Cell-Battery Powered Electric Vehicle

Susanta K. Das, Jinsu Kim

***Summary* — A MATLAB-Simulink based mathematical vehicle simulation model is developed in this investigation to analyze power management strategy of a proton exchange membrane (PEM) fuel cell and battery powered electric vehicle. The vehicle simulation model incorporated a real- world commercial passenger vehicle operator's drive cycle inputs and associated vehicle dynamics to determine accurate estimation of total onboard power requirements and withdrawal of power from the fuel cell and battery sources to meet the demand. The power management strategy is designed to meet the vehicle's onboard power demand based on the availability of hybrid combination of fuel cell and battery power sources. The fuel cell stack is the primary power source of the vehicle. Battery is used as a supplemental power source for meeting the vehicle's peak power demands. The fuel cell is also charging the battery with excess power produced onboard and hence controls the state-of-charge of the battery. All the important physical parameters are optimized to implement the power management strategy by considering the battery state-of-the charge, the drive torque and the vehicle drive performance. The model simulation results with optimized parameters showed that the power requirement of the electric vehicle was significantly affected by the combination of fuel cell and battery power management system as well as the vehicle operating behaviors of the end user (driver).**

***Keywords* — power management, fuel cell, battery, electric vehicle, model simulation.**

I. Introduction

Serious health problems for human life and environment pollution around the world have raised lot of concerns about the usage of fossil fuels based internal combustion engine (ICE) technology in transportation and other utilityvehicles[1]. Fuel cell and battery powered electric vehicles, as an alternative of ICE vehicles, have shown the most promising among others for zero to low greenhouse gas emission, high efficiency and long operational life[2].To improve the dynamics and uninterrupted power supply issues for the smooth operation of electric vehicles, a hybridization of fuel cell system (FCS) with an energy storage device such as lithium-ion battery pack can be a beneficial system. Hybridization is also helpful to achieve better fuel economy and performance by the optimization of fuel-cell and battery power sharing system. Through a power management strategy (PMS) based on the vehicle operating behaviors of the end users i.e. drivers, the optimization of this hybrid system is accomplished by distributing the load power between the fuel cell stack and batterypack. The design of such a PMS should be made by ensuring that each energy source operates within its limits to achieve an optimal fuel economy. The primary objectives of this investigation are to evaluate a power management strategy through implementation in a fuel cell and battery electric vehicle simulation model.

Even though fuel cell and battery powered electric vehicles (FCBPEVs) have not yet entered into the nationwide commercialization phase in large scale, fuel cell and battery powered electric vehicles have a great potential to be the most efficient environment friendly vehicles in the transition of the transportation sector [3]. FCBPEVs are characterized where a fuel cell stack acts as the main power source and a battery as an auxiliary energy storage device (AESD) to supplement the electric vehicle's peak powerdemandas needed [4]. Instead of a full fuel cell stack based powertrains, to form a hybrid powertrain mode by adding anAESD is advantageous: (1) since initially the FCS requires a little bit long start-up times due its slow electro-kinetics; hence an AESD is needed to starting up and also to improve the responsiveness of the peakpower demand during vehicle acceleration; (2) in the hybrid fuel cell and battery system, the fuel cell stack needs to be sized according to the cruising demand only since the AESD helps meet the peak power demands; (3) the AESD is also significantly improve the fuel economy by restricting the FCS to operate at a high-efficiency operating point and also leave the option open for the possibility of adding a regenerative braking system. For electric vehicles application, the hybrid fuel cell and battery system are required to achieve a minimum operational life time of 5000h [5] in orderto be comparable with the current internal combustion engine (ICE) based automotive powertrains.

Because of differences in their characteristics, multiple powersources involved in the hybrid powertrain affect electric vehicle performance considerably [6-7]. In the FCS, load changing characteristic leads to many degradations such as membrane dehydration, flooding of the porous electrodes' media and gas starvation causes the loss in the catalyst layer [8]. Hence, to increase the FCS lifetime, the FCS load dynamics need to be adjusted accordingly. On the other hand, battery lifetime depends on the depth-of-discharge as well as the charge-discharge rate of the battery. The discharge capacity of the battery usually decreases due to increase in the internal resistance as the battery aging [9]. Also, the battery operating conditions contribute significantly in cycle life of the battery.

Hence, to achieve optimal performanceand maximum fuel economy for FCBPEVs, power management strategy must be determined to accurately sizing the fuel cell stack and battery pack. Inthis study, we analyze the powermanagement strategy of a fuel

(Corresponding author: Susanta K. Das).

Susanta K. Das is with the Mechanical Engineering Department, Kettering University, Flint, MI 48504 USA (e-mail: sdas@kettering.edu).

Jinsu Kim is with the Mechanical Engineering Department, Kettering University, Flint, MI 48504 USA (e-mail: kim3045@kettering.edu).

Susanta K. Das, Jinsu Kim, Power Management Strategy of a PEM Fuel Cell-Battery Powered Electric Vehicle, Journal of Energy, vol. 72 Number 4 (2023), 3–8
https://doi.org/10.37798/2023724499

cell-battery powered electric vehicle by employing MATLAB and Simulink model. A mathematical FCBPEV simulation model was designed and using MATLAB and Simulink we optimized various physical model parameters to understand the power management strategy.

II. Simulation Model Description and methods

In this study, a mathematical FCBPEV simulation model is designed by considering the actual real-world vehicleo peration point of view. Figure 1 shows an overall vehicle simulation model diagram. The complete vehicle simulation model is comprised of six parts: drive cycle source, driver block,energy management system (EMS) block, electrical subsystem block, driveline block, and vehicle dynamics block. Using the MATLAB and Simulink software package [10], major vehicle components and control strategies were designed in each individual subsystem block and connected to each other to form a complete vehicle simulation model. The mathematical model equations used for the fuel cell stack in this study are given in our earlier publication [11] and the battery pack model equations provided in the publications [12-13] were used in the present Matlab-Simulink model simulation study.

The simulation model starts with a driver block that determines the acceleration required to achieve desired vehicle speed from the drive cycle source and provides it to the EMS block in the form of pedal position. The EMS block then calculates the reference torque of the electric motor and the reference current of the fuel cell based on an implemented control strategy [14]. With the reference torque values, the hybrid power train in the electrical subsystem block determines the actual motor torque and calculates required power based on the reference current load from the fuel cell stack. The vehicle's tractive force is then determined through the driveline block and the actual vehicle speed is calculated from the relationship between the road load force and the tractive force in the vehicle dynamics block.

The vehicle simulation model was optimized by implementing the power management mechanism and different operating conditions to understand the effect of various parameters on the overall vehicle performance. The designed vehicle simulation model was simulated by employing two types of driving cycles that are commonly used in the United States (U. S.) - the Urban Dynamometer Driving Schedule (UDDS) and the Highway Fuel Economy Test (HWFET) Driving Schedule to understand the power sharing mechanism of a FCBPEV. These two driving schedules, UDDS and HWFET, are parts of various drive cycles established by the U.S. Environmental ProtectionAgency(EPA) [15]. The U.S. EPA has published fuel economy test data of millions of new vehicles sold in the U. S. since late 1970s. UDDS describes a standard city driving pattern represented by frequent stops and go's. Whereas, unlike the city test, HWFET keeps the vehicle speed consistently in the range of 45 to 70 mph with the minimum usage of brakes.

A fuel cell-battery electric vehicle usually utilizes a fuelcell system as the main power source and a battery pack as the auxiliary power

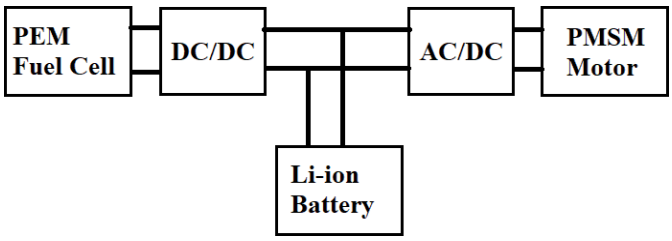

Fig. 2. EMS Block and electrical subsystem block for a fuel cell-battery hybrid powertrain system

source because the fuel cell alone may not be enough to satisfy all dynamic load demands in real-time vehicular applications [16]. Thelithium-ion batterypack in the model acts as an auxiliary power source to assistthe PEM fuel cell stack power supply as well as it also acts as an energy storage system to store produced surplus fuel cell energy or even restore the energy from regenerative braking as every time vehicle stops and start, it turns kinetic energy into electricity that is used to charge the battery and improve the system efficiency. Since the fuel cell stack voltage is higher than the dc bus voltage, a step-down DC/DC converter (or sometimes called a buck converter) was connected to the fuel cellsystem. One of the main challenges for the development of a hybrid electric vehicle is the management of multiple power sources and converters [17-18]. For a vehicle with hybrid power train, therefore, a power management strategy is required to accurately distribute the power between different power sources.Theenergymanagementsystem(EMS) blockcontains the power management strategy as well as the drive torque/power calculation block. In this study, The Energy Management Subsystem (EMS) block and the Electrical Subsystemblock were adapted from MATLAB/Simulink Sim-Power Systems library [10]. A diagram of the fuel cell-battery hybrid power train implemented in the EMSblock and electrical subsystem block is provided in Fig. 2.

In this study, the EMS and electrical subsystem shown in Fig. 2 consists of [10, 14]:

- A 100-kW permanent magnet synchronous motor (PMSM) with maximum torque of 256 N.m and maximum speed of 12,500 rpm.
- A 25kW, 288Vdc ,86.8Ah lithium-ion battery pack.
- A 100kW, 288Vdc proton exchange membrane(PEM) fuel cell stack.
- A step-down DC/DC converter.

It is noted that, in this study, an electric motor has been treated as the power source (i.e. heat engine) that is the closest to the ideal power plant because of the constant power output over the high-speed range and the constant torque output over the low-speed range [1]. Unlike the conventional gasoline engine, the electric motor used in the fuel cell-battery electric vehicle can produce torque at zero speed and efficiency of power plant is less dependent on

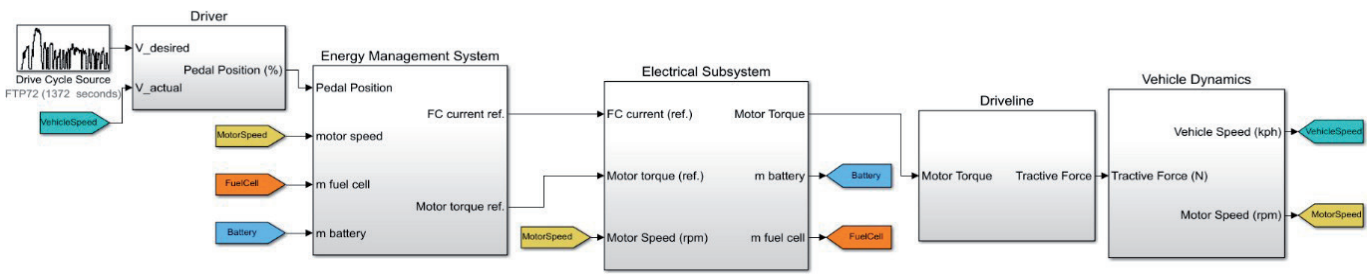

Fig. 1. MatLab-Simulink based fuel cell-battery powered electric vehicle (FCBPEV) simulation model

Susanta K. Das, Jinsu Kim, Power Management Strategy of a PEM Fuel Cell-Battery Powered Electric Vehicle, Journal of Energy, vol. 72 Number 4 (2023), 3–8
https://doi.org/10.37798/2023724499

its operating points. Due to this ideal torque-speed profile, a single-gear transmission is commonly used for the vehicle with the electric motor.

The battery management system shown in Fig.2 determines the battery State of Charge (SOC) limit and the battery power limit as well as the battery recharged power based on the measured voltage and SOC. The power management system then determines the reference motor torque and the reference fuel cell current based on the battery recharge power and the batterylimits calculated from the battery management system.

The model simulation starts with the torque calculation block, shown in Fig. 1, that calculates the drive torque and drive power using the pedal position and motor torque-speed relationship. In order to convert the motor speed to motor torque, peak performance curve of the motor was generated using the maximum torque, speed, and power demand values of the motor. The reference fuel cell power is calculated by adding the battery recharge power to drive power. The drive power is described as a subtraction in the block (see Fig. 1) because the recharge power is usually expressed as negative value by convention. The reference fuel cell stack current is then determined using the polarization curve of the fuel cell stack. The reference Battery Power block determines the behavior of the battery using the reference fuel cell power, measured fuel cell power, battery recharge power, and the battery power limit. The battery power block commands the battery to help the fuel cell when the fuel cell alone cannot provide the required drive power to the motor. Since the fuel cell system cannot react quickly, due to its long response time at pre-start, the switch block is used to ensure that the battery power kicks in while the fuel cell system heats up at the time of start of the vehicle.

The driveline block, shown in Fig. 1, converts the motor torque produced by the electric motor considering the tractive effort on the wheels. The torque of the power plant such as an engine or an electric motor is, in general, transmitted to the wheels through a clutch in manual transmission or a torque converter in automatic transmission, gearbox, final drive, differential, and drive shaft. The driveline block is also considered the traction limit. When the tractive resistance of a vehicle exceeds the limit of the maximum tractive force due to the friction between the tire and the ground, the vehicle cannot go forward and the wheels will spin on the ground. For the accuracy of the simulation, therefore, the tractive limit due to the friction has been taken into consideration. The vehicle dynamics block calculates the vehicle speed using the tractive force estimated from the vehicle dynamics block, see Fig. 1. Using the tractive force, the power required from the motor to propel the vehicle moving forward at a specific speed can be determined.III.

III. Results and Discussions

To verify the power management strategy embodied in the Energy Management System (EMS) block, first, the vehicle model was simulated with a series of step input signals to verify the pedal position at different scenarios. The baseline vehicle model is then validated by running the simulation with the two drive cycles (UDDS and HWFET) and analyses the results in terms of power sharing mechanism with a certain amount of vehicle driving distance.

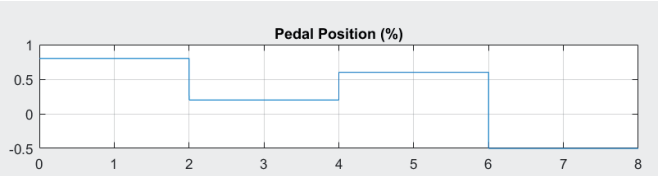

Fig. 3. Pedal position step input signal validation

In order to understand the power sharing mechanism, the vehicle model is simulated with a series of step input signals, after verification of pedal position, that describes different modes of operation such as fast acceleration, gentle acceleration, and braking [14] to verify that the power management strategy implemented in the EMS block properly controls the power sources at different scenarios. Fig. 3 represent a series of four step input signal for power control strategy validation describes the following operational management strategy implemented in the EMS block properly controls the power sources at different scenarios. Fig. 3 represent a series of four step input signal for power control strategy validation describes the following operational behaviors: (a) the accelerator pedal is pushed to 80% (fast acceleration), (b) the accelerator pedal is released to 20% (gentle acceleration), (c) the accelerator pedal is pushed again to 60% (fast acceleration), (d) the brake pedal is pushed to 50% (deceleration).

For the baseline vehicle model, the values of vehicle dynamics and driveline parameters have been estimated based on the generalized use of the vehicle as shown in Table I.

TABLE I
Vehicle Dynamics Parameters of the Baseline Vehicle.

Parameter	Value
Vehicle mass, m	1800 kg
Width of vehicle, W	1.85m
Height of vehicle, H	1.50m
weight distribution, $i_{WD,f}/i_{WD,r}$	0.52/0.48
Tire dynamic radius, r_d	0.315m
Single gearset ratio, igi 0	8:1
Driveline efficiency, η_t	0.90
Friction coefficient (dryroads), μ	0.75
Tire dynamic radius, r_d	0.315m
Drag coefficient, C_d	0.3
Rolling resistance coefficient, f_{rr}	0.015
Incline angle, θ	0 (level ground)
Mass factor, k_m	1.05

After validation of pedal position with the step input signal, as shown in Fig. 3, the driver block and drive cycle block from the vehicle simulation model, as shown in Fig. 1, were replaced with the pedal position signal block and hence the signal input was regarded as the pedal position and directly connected to the EMS block [14]. Hence, it makes the vehicle simulation mode more robust and forged coupling of vehicle speed, battery SOC, and power distribution between battery and fuel cell depending on the pedal position input.

Susanta K. Das, Jinsu Kim, Power Management Strategy of a PEM Fuel Cell-Battery Powered Electric Vehicle, Journal of Energy, vol. 72 Number 4 (2023), 3–8
https://doi.org/10.37798/2023724499

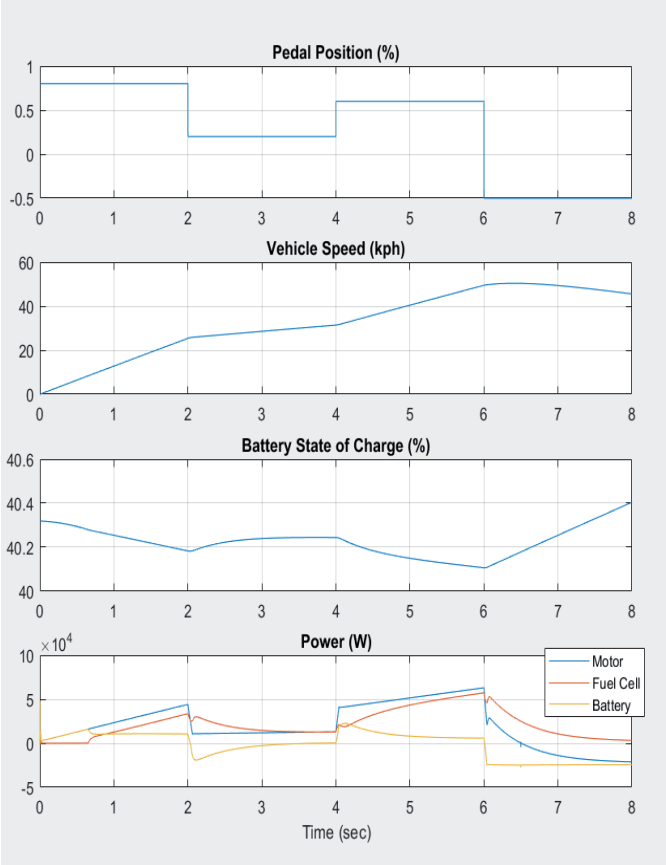

Fig. 4. Vehicle speed, battery SOC and power distribution curves of fuel cell and battery based on the pedal position

Fig. 4 shows the vehicle model simulation results of vehicle speed, battery SOC, and power distribution curves of battery and fuel cell depending on the corresponding pedal position input. The pedal position signal consists of a series of four step inputs: 80% at 0 s, 20% at 2 s, 60% at 4 s, and -50% at 6s. the negative accelerator input is regarded as the brake pedal position. From Fig. 4, it can be seen that at time t = 0, the vehicle is at idle (stopped) position and the driver pushes the accelerator pedal to 80% (fast acceleration). At this situation, the battery alone provides the power to the motor until the fuel cell starts to provide the power. The vehicle speed steadily goes up and the battery power is also depleted rapidly as can be seen from Fig. 4. At 0.7 seconds, the fuel cell starts to provide power to the motor as a main power source while the battery continues to provide power as an auxiliary power source to meet the motor power demands. At 2 seconds, the accelerator pedal is released to 20% (gentle acceleration). Now, the fuel cell solely provides the power and battery power goes to zero. As the accelerator pedal is pushed hard to 60% (fast acceleration) at 4 seconds, the battery kicks in again and start to help the fuel cell stack to realize the power demand. Then the driver pushes the brake pedal to 50% at 6 seconds. The motor acts as a generator now and restore the fuel cell excess energy into the battery by charging it through regenerative braking system. The battery SOC starts to increase as the battery energy is restored. It can be concluded from the results presented in Fig. 4 that the power was successfully distributed and shared between the battery and the fuel cell as initially intended by the energy management system (EMS) block. Hence, the power management strategy applied in the EMS block was validated and found to be worked properly.

The vehicle simulation model was run with UDDS (city) schedules for 1400 seconds and HWFET (highway) driving schedules for 800 seconds to understand the power sharing mechanism between power providing sources - fuel cell and battery during the city driving and highway driving conditions.

Fig. 5 represents the vehicle speed, drive torque and power sharing curves during the city driving using city driving schedule. From Fig. 5, it can be found that the maximum drive torque is measured as around 180 Nm during the city driving test. Since the torque was maintained below the maximum torque of the motor

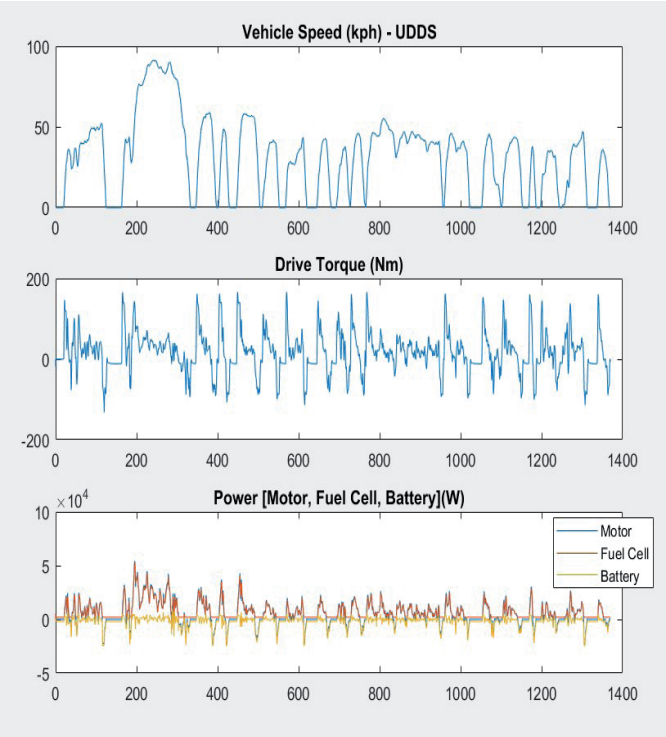

Fig. 5. Vehicle speed, drive torque and power distribution curves of fuel cell and battery on City driving test

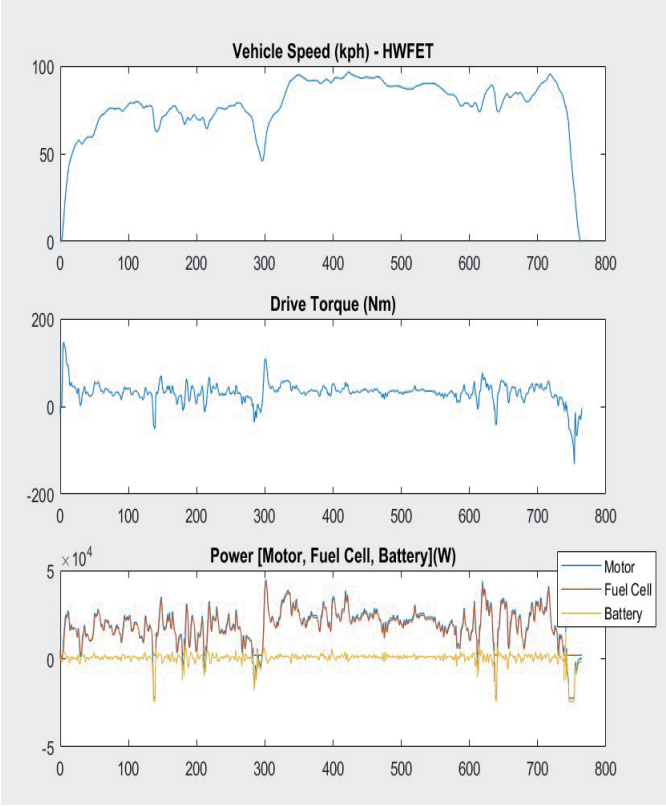

Fig. 6. Vehicle speed, drive torque and power distribution curves of fuel cell and battery on Highway driving test

Susanta K. Das, Jinsu Kim, Power Management Strategy of a PEM Fuel Cell-Battery Powered Electric Vehicle, Journal of Energy, vol. 72 Number 4 (2023), 3–8
https://doi.org/10.37798/2023724499

of 256 Nm during the whole cycle, the fuel cell only provided the required power to the motor for most of the time and the battery mainly acts as an energy storage during this test. As can be seen from Fig. 5, the negative torque profile appears a lot because of frequent stops in the city test. This leads to a frequent battery charging due to regenerative braking. The maximum fuel cell power was measured as 52 kW while the maximum battery power was only measured as 3 kW. From Fig. 5, it can also be seen that since the city driving is limited mostly within 50 km/h, the fuel cell power source was provided the required power most of the times and the battery storage the excess power produced by the fuel cell as indicated by the negative spike of power curves for the battery during the city driving. For an instance of high vehicle speed during the city driving between 200-350 seconds, as shown in Fig. 5, it can be seen that the battery power supplemented the power to the fuel cell power in order to meet the additional power needed for high speed city driving. This can be clearly seen from Fig. 5 as the negative power spikes diminished for battery power curve during the high-speed city driving between 200-350 seconds. It clearly demonstrated the power sharing and power saving mechanism during the city driving as the power management strategy incorporated nicely in the developed vehicle simulation model in this study.

Fig. 6 represents the vehicle speed, drive torque and power sharing curves during the highway driving using the highway driving schedule. From Fig. 6, it can be seen that the maximum drive torque was measured as around 150 Nm during the highway driving test. Similar to the city driving test, the torque stayed below the maximum torque of the motor of 256 Nm during the entire highway driving cycle. From Fig. 6, it can be seen that the fuel cell power source was mostly provided the power to the motor and the battery power supplemented to meet the peak power demand only and the battery was acted as an energy storage very less frequently as very few negative power spikes displayed by the battery power curves during the highway driving test. The maximum fuel cell power was measured as 45 kW while the maximum battery power was measured as 2.3 kW. From Fig. 6, it is also seen that there are very few negative torque spike curves due to the fact that the vehicle is driven most of the times above the speed of 50km/h and less frequent stops because of no traffic light at the highway. From Fig. 6, it was found that when the vehicle speed was very high, for instance, highway driving time between 300-600 seconds, the required motor power was supplied by the fuel cell system and the battery as can be seen from Fig. 6, During this time, 300-600 seconds, the battery power curves show almost no negative spike instead it shows frequent small positive spikes. It indicated that during the high vehicle speed at the highway driving, the battery mostly supplemented the power with fuel cell power to fulfill the peak power demand of motor to maintain the same high speed during 300-600 seconds as can be seen from Fig. 6, It also found that the vehicle's drive torques were almost remained the same during the highway driving periods 300-600 seconds. Overall, from Fig. 6, it can be seen that the vehicle speed, drive torque and power sharing between the fuel cell and battery power sources were correlated excellently as expected in the developed vehicle simulation model.

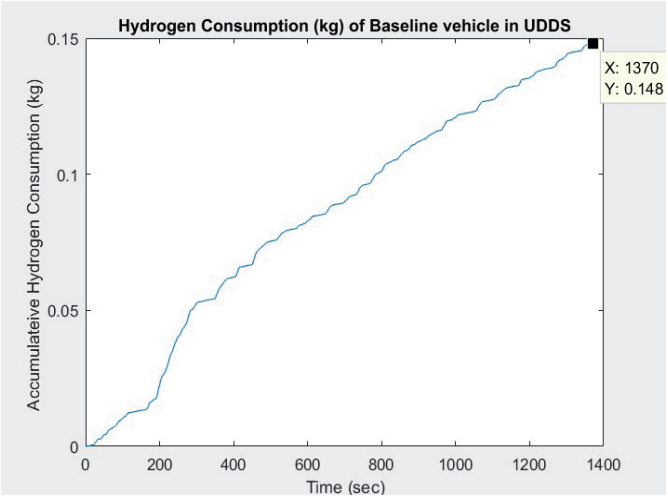

Fig. 7. Amount of hydrogen consumption during City driving test of fuel cell–battery electric vehicle

Fig. 7 represents the amount of hydrogen consumption during the city driving test. The hydrogen consumption amount is calculated using the developed Mathlab-Simulink model of fuel cell-battery electric vehicle while used the city driving schedule. In the model, the hydrogen consumption rate of the fuel cell stack was calculated using the equation (1) give as [2]:

$$Hydrogen\ consumption\ \text{rate} = \frac{i_{fc} RTN}{2FP_{fuel} x\%} \qquad (1)$$

where i_{fc} is the fuel cell current, R is the ideal gas constant $\left(8.3145\ \frac{J}{mol\ K}\right)$, T is the operating temperature, P_{fuel} is the absolute supply pressure of fuel, N is the number of cells, F is the Faraday's constant $\left(96{,}485\ \frac{A\,s}{mol}\right)$, x is the hydrogen composition in the fuel.

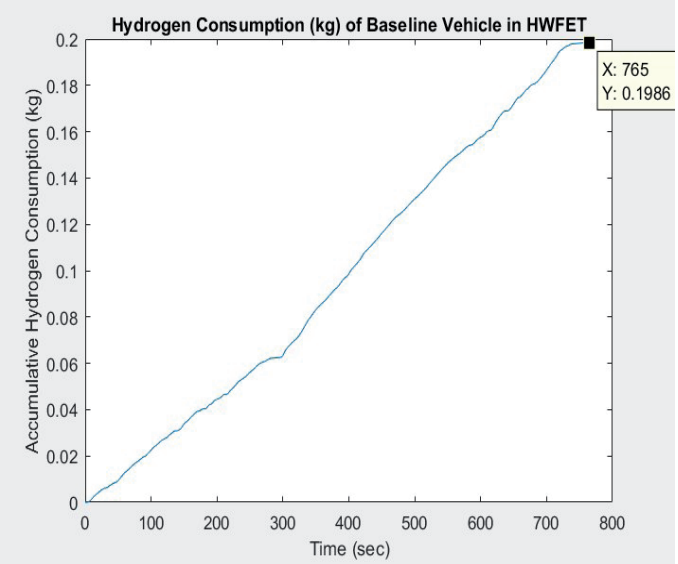

Fig.8. Amountofhydrogenconsumptionduring Highwaydriving test of fuel cell–batteryelectric vehicle

From Fig. 7, it can be seen that the total hydrogen consumption during the city driving cycle was about 0.148 kg during the total city driving time of 1370 seconds i.e. around 23 minutes. The average city driving speed was calculated at around 32 mile per hour. The total distance travel with the city driving schedule was around 12 miles and hence the city fuel economy rating was calculated as around 81 miles per kilogram of hydrogen used.

Fig. 8 shows the amount of hydrogen consumption during the Highway driving test of fuel cell-battery electric vehicle. The hydrogen consumption amount was calculated using equation (1) and employing the Matlab-Simulink model parameter values while using the Highway driving schedule. From Fig. 8, it is observed that the total hydrogen consumption during the total 765 seconds i.e. about 13 minutes of highway driving test using the Highway driving schedule was about 0.1986 kg. Total distance travel during

Susanta K. Das, Jinsu Kim, Power Management Strategy of a PEM Fuel Cell-Battery Powered Electric Vehicle, Journal of Energy, vol. 72 Number 4 (2023), 3–8
https://doi.org/10.37798/2023724499

the Highway driving schedule test was about 14 miles with around 65 miles per hour vehicle speed. Based on the collected data using the Highway driving schedule and driving test, the highway fuel economy rating was calculated as around 71 miles per kilogram of hydrogen used.

Comparing Figs. 7 and 8, it can be seen that the fuel economy rating is higher at the city driving than highway driving of the fuel cell-battery electric vehicle. The results show the usual trend for an electric vehicle compared to an internal combustion engine-based gasoline/diesel vehicle. Since the fuel cell-battery electric vehicle utilize regenerative braking system to recover lost energy due to frequent braking for traffic stops during city driving and hence the fuel economy rating is higher at city driving compared to highway driving due to no to less traffic stop on the highway driving. The conventional gasoline vehicles have higher highway fuel economy ratings than the city ratings because of large kinetic energy loss due to frequent braking for traffic stops during city driving. Based on the results presented in this study, it can be seen that unlike the conventional vehicles, fuel cell-battery electric vehicles have higher city fuel economy rating than the highway rating because of the braking energy is recovered through regenerative braking system.

IV. Conclusions

A Matlab-Simulink based complete vehicle simulation model of a fuel cell-battery powered electric vehicle was designed and simulated to understand the power management strategy of fuel cell and battery power supply sources. The developed vehicle simulation model was tested with two U.S. standard driving cycles such as city driving cycle (UDDS) and highway driving cycle (HWFET) to understand the underlying physics of fuel cell-battery electric vehicle's power management system. In the model simulation, it was assumed that the rechargeable battery pack was maintained appropriately to prevent over-heating and no loss of storage capacity degradation. It is also assumed that the water management system was put in place for the fuel cell stack to maintain the humidity inside the fuel cell at an appropriate level to prevent membrane dehydration. The results obatined in this study showed that the power management strategy implemented in the vehicle simulation model successfully distributed the power between the fuel cell and battery in both the city driving and highway driving conditions. The simulation results also showed that there is a strong correlation among vehicle speed, driving torque and power distribution mechanism in the fuel cell and battery powered electric vehicle. The results clearly showed that, unlike the conventional vehicles, fuel cell-battery electric vehicles have higher city fuel economy rating than the highway rating because of the lost braking energy for frequent traffic stops is recovered through regenerative braking system. The model simulation results provided an important insight and improved understanding in power management mechanism of a fuel cell and battery power electric vehicle. The knowledge gained in this investigation will definitely be useful for further exploration in a future study.

Acknowledgment

The author, Jinsu Kim, thanks the sponsored research office of Kettering University for providing a graduate research assistantship through an external research grant funding during accomplishing this research work.

References

[1] M. Ehsani, Y. Gao, S. E. Say and A. Emadi, "Modern electric, hybrid electric, and fuel cell vehicles: Fundamentals, theory, anddesign.,"CRC Press, 2005.

[2] F. Barbir, "PEM fuel cells: Theory and practice.,"Academic Press, 2013.

[3] S. Onori, L. Serrao and G. Rizzoni,"Hybrid electric vehicles: Energy management strategies," London: Springer, 2016.

[4] S. K Das and J. Kim,''Evaluation of power sharing mechanism of a PEMfuel cell-battery powered electric vehicle", Proc. 2023 4th International conference on Clean and Green Engineering (CCGE), held in Ankara,Turkey, August 26-28, IEEE Press, ISBN 979-8-3503-3978-8, p. 112- 117, 2023.

[5] J. Kim, "Power supply management of a fuel cell-battery hybrid electric vehicle, " M.Sc. thesis submitted to Kettering University, 2020.

[6] Y. Manoharan, S. E. Hosseini, B. Butler, H. Alzhahrani, B. T. Fou Senior, T. Ashuri and J. Krohn, "Hydrogen Fuel Cell Vehicles; Current Status and Future Prospect," Appl. Sci., vol. 9, pp. 2296-2314, 2019.

[7] S. E. Hosseini and B. Butler, "An overview of development and challenges in hydrogen powered vehicles," Int. J. Green Energy, vol. 17(1), pp.13–37,2020.

[8] J. Larminie and A. Dicks, "*Fuel cell systems explained*.," Chichester,West Sussex: J. Wiley, 2003.

[9] A. A. Kebede, T. Coosemans, M. Messagie, T. Jemal, H. A. Behabtu, J. V. Mierloand M. Berecibar, "Techno-economic analysis of lithium-ion and lead-acid batteries in stationary energy storage application," J. EnergyStorage, vol. 40, pp.102748-102767, 2021.

[10] MATLAB and Simulink R2023a, The MathWorks, Inc., Natick, Massachusetts, United States.

[11] S. K. Das and H. A. Gibson, "Threedimensional multi-physics modeling and simulation for assessment of mass transport impact on the performance of a high temperature polymer electrolyte membrane fuelcell", J. Power Sources, vol. 499, pp. 229844, 2021.

[12] D. Linden and T. B. Reddy edited, "Handbook of Batteries", 3rd Ed.,McGraw-Hill, New York, 2002.

[13] S. K. Das, A. Sarkar and K. J. Berry, "Experimental Performance Evaluation of a Hyper-Branched Polymer Electrolyte for Rechargeable Li-Air Batteries", J Front. Energy Res., vol. 8, pp. 00075, 2020. doi:10.3389/fenrg.2020.00075.

[14] S.N. Motapon, O. Tremblay, and L-A. Dessaint,"Development of a generic fuel cell model: application to a fuel cell vehicle simulation.,"Int. J. Power Electronics,*vol.*4(6),pp.505-522,2012.

[15] Data on Cars used for Testing Fuel Economy. (n.d.). U. S. Environmental Protection Agency. Retreived fromhttps://www.epa.gov/compliance-and-fuel-economy-data/data-cars-used-testing-fuel-economy

[16] H. Yang, Y. J. Han, J. Yu, S. Kim, S. Lee, G. Kimand C. Lee,"Exploring future promising technologies in hydrogen fuel cell transportation," J. Sustainability, vol. 14, pp. 917-936, 2022.

[17] S. N. Motapon, L.-A. Dessaint, and K. Al-Haddad,"A comparative study of energy management schemes for a fuel-cell hybrid emergency powersystem of More-Electric aircraft," IEEE Trans. Ind. Electronics, vol.61(3), pp. 1320-1334, 2014.

[18] S. N. Motapon, O. Tremblay and L.-A. Dessaint, "A generic fuel cellmodel for the simulation of fuel cell power systems," Power & EnergySociety General Meeting, pp. 1-8, 2009.

Susanta K. Das, Jinsu Kim, Power Management Strategy of a PEM Fuel Cell-Battery Powered Electric Vehicle, Journal of Energy, vol. 72 Number 4 (2023), 3–8
https://doi.org/10.37798/2023724499

Journal of Energy
VOLUME 72 Number 4 | 2023
journal homepage: http://journalofenergy.com/

Application of Adaptive Finite Focus Beamforming Method for Localization of Low-frequency Transformer Sound

Karlo Petrović, Antonio Petošić, Tomislav Župan

***Summary* — In this paper, the developed adaptive linearly constrained minimum variance finite focus beamforming method is used to increase the accuracy and resolution of low-frequency transformer sound source localization. In the first step, simulations on virtual arrays are conducted to define the array size and compare the influence of three different beamforming algorithms on sound localization accuracy and resolution. In the second step, measurements of the regulating transformer as a noise source are conducted in the semi-anechoic chamber. A large rectangular microphone array, with 90 microphone positions spaced 0.44 meters apart, is used for that purpose. The developed algorithm is compared with infinite and finite focus beamforming for the localization of total noise and noise at specific noise harmonics.**

***Keywords* — finite focus beamforming, adaptive beamforming, rectangular microphone array, regulating transformer.**

I. Introduction

The conventional beamforming technique for sound source localization in acoustic cameras is applicable in far-field and at higher frequencies, mainly above 500 Hz. However, dominant frequency components of transformer noise are often below that frequency. The problem is highlighted in the literature [1], [2], and [3], where an acoustic camera is used for the localization of low-frequency transformer sound. The hotspot localization results show low spatial resolution in the frequency range below 300 Hz. That makes the method inapplicable for localizing sound sources in a transformer. Instead, knowing the exact distance from the source to the beamforming array, a finite-focus method [4] can be applied. Additionally, adaptive beamformers [5] can be used by choosing weights based on the statistics of the received data.

Besides beamforming, there are three significant sound source localization techniques: nearfield acoustic holography (NAH), statistically optimized nearfield acoustic holography (SONAH), and direct acoustic intensity measurements. Another noise source identification technology that combines the far-field beamforming method with the near-site acoustic holography can be applied to the transformer for a higher resolution [6]. The application of direct acoustic intensity measurements to localize noise on 16 MVA and 75 MVA transformers is explained in [7] and [8], respectively.

This study pointed out the possibility of the beamforming met hod application for localizing low-frequency transformer sound. The motivation for the work is to develop an easily applicable and accurate method with high resolution at low frequencies at which the transformer operates. A simple application of the method is achieved with only one microphone and the possibility of measurement automatization without requiring measurements at very short distances from the surface, as in [6–8]. Sound localization accuracy is achieved using an unconventional finite-focus method, and increased resolution is achieved using an adaptive beamformer, thus avoiding the conventional acoustic camera problems [1-3]. Compared to the previous research, this work developed a new, improved method that needs only one microphone and combines finite-focus and adaptive beamforming with a known distance from the source to localize low-frequency sound.

In the paper, a brief overview of the beamforming theory is given. The three different beamforming algorithms are simulated on the specified microphone array. A wooden frame for positioning microphones along the beamforming array is presented, and the measurement procedure is described. Analysis of the measurement in the semi-anechoic room is carried out. In the end, conclusions and suggestions for future research are given.

II. Theoretical Background

In the beamforming technique, the amplitude and the phase of the sound pressure over an array of microphones are measured. The technique maximizes the total summed output for the sound coming from the specified direction while minimizing the sound coming from another direction. It is used in the far field of the sound source and is more suitable for higher frequencies. The frequency and the dynamic range of beamforming measurements depend on the array type and size. The beamforming has the disadvantage of low spatial resolution in localizing a noise source, especially at low frequencies. The advantage is that it can image distant and moving sources. The two types of beamforming are infinite-focus distance and finite-focus distance beamforming.

A. Infinite focus beamforming

The plane waves are assumed for the infinite focus beamforming, and the spherical waves are assumed for the finite focus beamforming. Beamforming theory is explained in more detail in

(Corresponding author: Karlo Petrović)
Karlo Petrović and Tomislav Župan are with the Končar - Electrical Engineering Institute Ltd., Zagreb, Croatia (e-mails: kpetrovic@koncar-institut.hr, tzupan@koncar-institut.hr)
Antonio Petošić is with the University of Zagreb, Faculty of Electrical Engineering and Computing, Zagreb, Croatia (e-mail: antonio.petosic@fer.hr)

Karlo Petrović, Antonio Petošić, Tomislav Župan, Application of Adaptive Finite Focus Beamforming Method for Localization of Low-frequency Transformer Sound, Journal of Energy, vol. 72 Number 4 (2023), 8–14
https://doi.org/10.37798/2023724507

[4], [9]. If the planar array consists of L microphones at locations $(x_l, y_l, l = 1, ..., L)$ in the x-y plane, and the measured signals p_l are individually delayed and then summed, the output of the array is:

$$p(\boldsymbol{n}, t) = \sum_{l=1}^{L} w_l p_l\big(t - \Delta_l(\boldsymbol{n})\big) \tag{1}$$

where w_l is the weighting coefficient, which reduces the importance of the signals coming from the array edges. The quantity $\boldsymbol{n}$ is the unit vector in the direction of the maximum sensitivity of the array, and the time delays Δl are chosen to maximize the array sensitivity in the direction $\boldsymbol{n}$, and it is defined as:

$$\Delta l = \frac{\boldsymbol{n} \cdot \boldsymbol{r}_l}{c} \tag{2}$$

where the vector $\boldsymbol{r}_l = (x_l, y_l)$ and the c is the speed of sound. The output of the beamformer in the frequency domain analysis at angular frequency ω is:

$$P(\boldsymbol{n}, \omega) = \sum_{l=1}^{L} w_l P_l(\omega) e^{-j\omega\Delta_l(n)} = \sum_{l=1}^{L} w_l P_l(\omega) e^{-j\boldsymbol{k}\cdot\boldsymbol{r}_l} \tag{3}$$

where $\boldsymbol{k} = -k\boldsymbol{n}$ is the wave number vector of a plane incident from the direction $\boldsymbol{n}$. The beamforming in the frequency domain provides the possibility to process independent frequencies. It is less computationally intensive and more suitable for steady-state situations. The time domain beamforming is more suitable for rapidly changing environments.

B. *Finite focus beamforming*

Finite-focus beamforming, assuming a spherical wave, follows a similar analysis. The various microphone delays should align for the array to focus on a point source at a finite distance. Equation (3) still applies, but the delay Δl is defined as:

$$\Delta l = \frac{|\boldsymbol{r}| - |\boldsymbol{r} - \boldsymbol{r}_l|}{c} \tag{4}$$

where $\boldsymbol{r}$ is the vector location of the source from an origin point in the same plane as the array, $\boldsymbol{r}_l$ is the vector location of microphone l in the array with respect to the exact origin, and $|\boldsymbol{r} - \boldsymbol{r}_l|$ is the scalar distance of microphone l from the source. An example of the beamforming localization principle is shown in Figure 1.

C. *Adaptive linearly constrained minimum variance beamforming*

A principle of adaptive beamforming is that the weights are chosen based on the statistics of the received data so that the signal-to-noise ratio (SNR) can be improved. That approach enables distinguishment between desired and interference signals. A linearly constrained minimum variance (LCMV) beamforming is first introduced in [10]. The algorithm is based on the minimum mean square error used to determine array weights. The optimal weights of the LCMV beamformer are calculated as follows [9]:

$$\boldsymbol{w}_{opt} = S^{-1}C(C^H S^{-1} C)^{-1}\boldsymbol{R} \tag{5}$$

where S is the sum of the noise and interference covariance matrix, C is the constraint matrix, H is the transpose conjugate of a vector, and $\boldsymbol{R}$ is the signal gains due to the constraint.

The advantages of the LCMV beamforming are that it has higher spatial resolution than the conventional beamformer, it is nulling in the direction of interference sources, sidelobes are smaller than in the conventional beamforming, and it only requires the direction of arrival to maximize SNR. Disadvantages are low convergence rate and susceptibility to self-nulling.

III. Methodology And Measurement

Three different algorithms are tested in this work:

- Infinite focus (IF) beamforming (conventional)
- Finite focus (FF) beamforming
- Finite focus (FF) adaptive beamforming (developed)

A. *Testing Algorithms on a Virtual Array*

A virtual array of 9×10 microphones is created in MATLAB, as shown in Figure 2. The distance between microphones is set to 0.44 m. The total size of an array is 3.56 m in height and 4 m in length. The size is selected so that the wooden frame with holes for microphone positions can be placed in a semi-anechoic chamber for experimental verification.

Simulated point sound sources are located at a finite distance of 2 m. The first source is at 100 Hz at the spherical coordinates [30°, 20°]. The second source is at 300 Hz at coordinates [-20°, 0°]. Spherical coordinates are marked as [azimuth, elevation]. The amplitude of simulated sound pressure is set to 0.1 Pa, in decibels equal to 70.97 dB RMS.

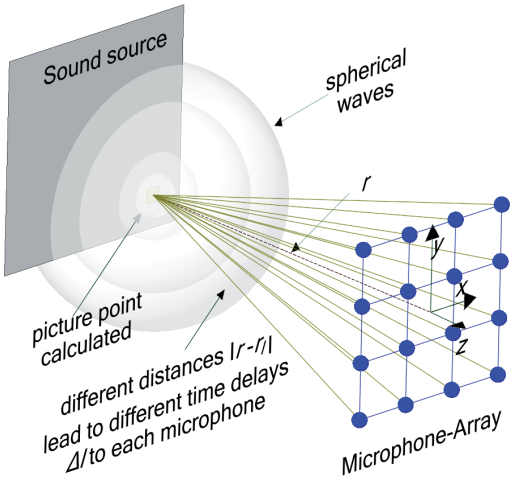

Fig. 1. Finite-focus beamforming localization principle

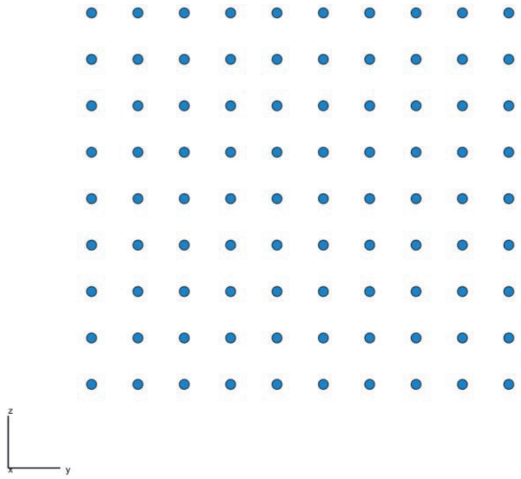

Fig. 2. Virtual array of 90 microphones in MATLAB

Karlo Petrović, Antonio Petošić, Tomislav Župan, Application of Adaptive Finite Focus Beamforming Method for Localization of Low-frequency Transformer Sound, Journal of Energy, vol. 72 Number 4 (2023), 8–14
https://doi.org/10.37798/2023724507

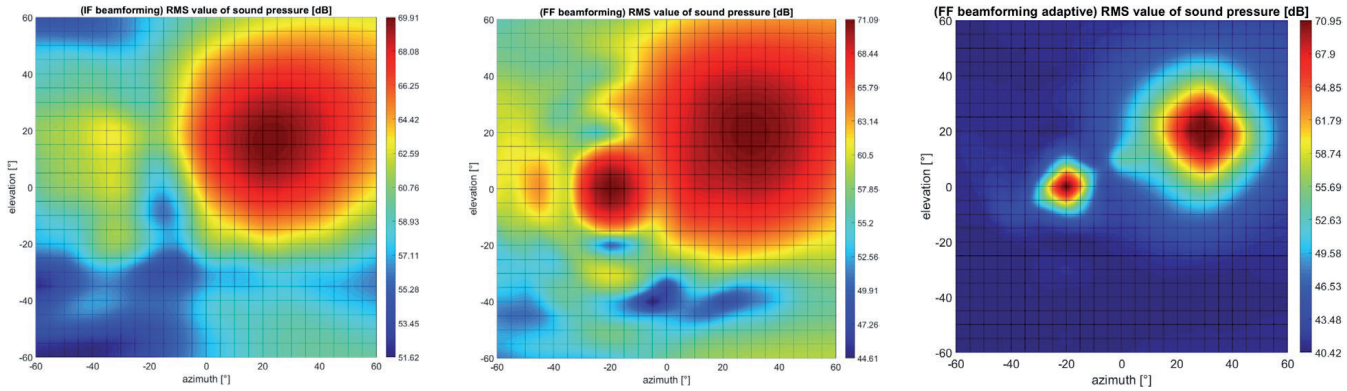

a) b) c)

Fig. 3. Localization of two simulated sound sources at a distance of 2 meters using a) infinite focus beamforming, b) finite focus beamforming, c) finite focus adaptive beamforming

Localization of two simulated sound sources from specified angles using IF beamforming and FF beamforming is shown in Figure 3a and 3b. Application of IF beamforming for the finite distance point source decreases localization accuracy. The 300 Hz source is not localized, and the coordinates of the 100 Hz source are localized with an error. The center of the source is located at approximately [22°, 17°] instead of assigned [30°, 20°].

FF beamforming does not increase the spatial resolution. It is roughly the same for both algorithms by comparing localizations of the 100 Hz source. On the other hand, localization accuracy compared to the IF beamforming is higher. The sources are localized at the exact coordinates.

A higher resolution is achieved by using a developed adaptive FF beamforming algorithm. Compared to the conventional FF beamforming algorithm, spatial resolution is increased, as shown in Figure 3c.

B. Measurement Procedure in the Semi-Anechoic Chamber

Measurements are conducted in the semi-anechoic chamber on the regulating transformer as a noise source. The dimension of the transformer is 1.3 m in width, 1.3 m in length, and 1.6 m in height.

Table I.

Nominal Data Of The Regulating Transformer

Rated power	160 kVA
Rated output voltage	0-500 V
Rated output current	185 A
Frequency	50 Hz
Number of phases	3
Mass	1150 kg

The measurement procedure consisted of a total of 18 measurements. Five sound pressure and voltage signals are recorded in each measurement using an acquisition card and laptop with B&K software. A voltage transformer is used to lower the voltage in order to measure it using an acquisition card. The measurement setup diagram is shown in Figure 4c.

A voltage signal aligns pressure signals as if measured at the exact moment. This technique enables the application of the beamforming algorithm without having 90 microphones for each measurement position. The regulating transformer is measured at 2 m from the source and 2.5 m from the source. Two different distances are used as the criteria to validate the method. The sound source should be localized at the exact coordinates regardless of the distance.

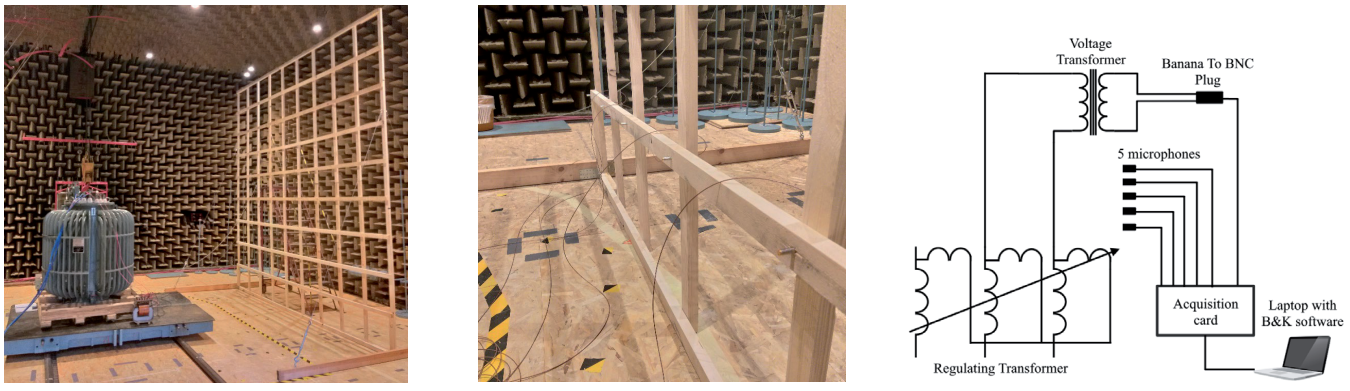

a) b) c)

Fig. 4. a) Regulating transformer and a wooden frame for a beamforming array in a semi-anechoic chamber b) placement of microphones used for measurements of sound pressure c) measurement setup diagram

Nominal data of the regulating transformer are given in Table I. The measurement setup with the regulating transformer and the wooden frame is shown in Figure 4a. Construction for a beamforming array consists of a total of 90 holes. Five microphones used for sound pressure measurements are shown in Figure 4b.

IV. Results

Voltage signals of all 18 measurements and sound pressure signals of 18 microphone measurements at the first position before alignment are shown in Figures 5a and 5c, respectively. The same signals after the alignment are shown in Figures 5b and 5d. The figure shows that the voltage signal is used as a reference signal,

Karlo Petrović, Antonio Petošić, Tomislav Župan, Application of Adaptive Finite Focus Beamforming Method for Localization of Low-frequency Transformer Sound, Journal of Energy, vol. 72 Number 4 (2023), 8–14
https://doi.org/10.37798/2023724507

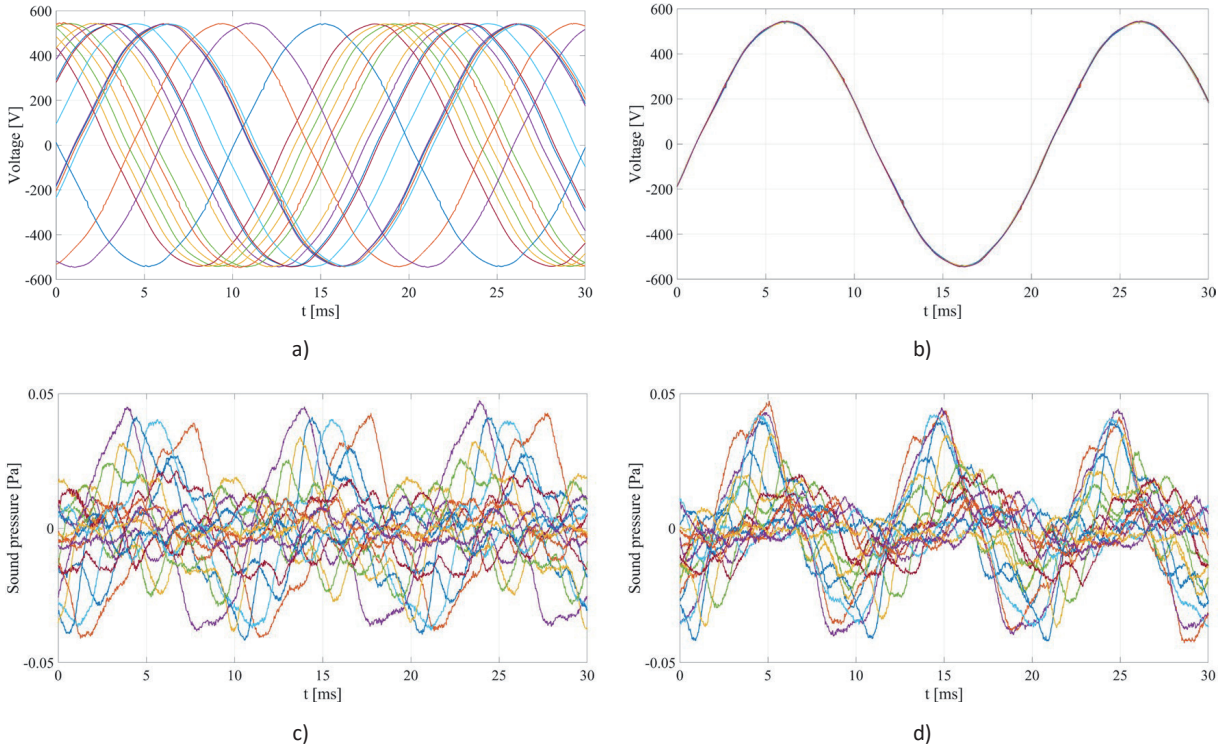

Fig. 5. a) Voltage signals of all 18 measurements before alignment b) after alignment c) sound pressure signals of microphone 1 of all 18 measurements before alignment d) after alignment

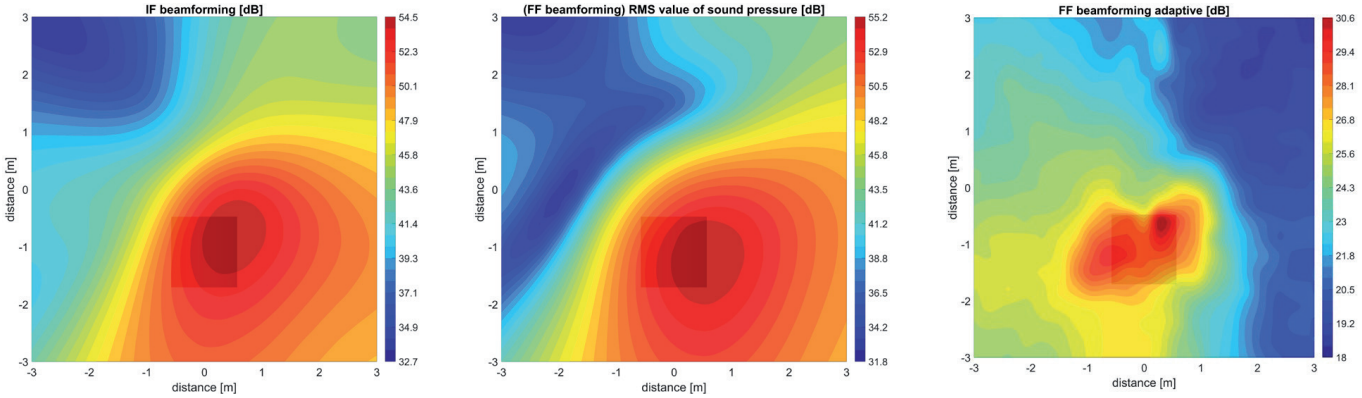

Fig. 6. Localization of regulating transformer noise at a distance of 2 m from the source using a) conventional infinite focus beamforming, b) finite focus beamforming, c) finite focus adaptive beamforming

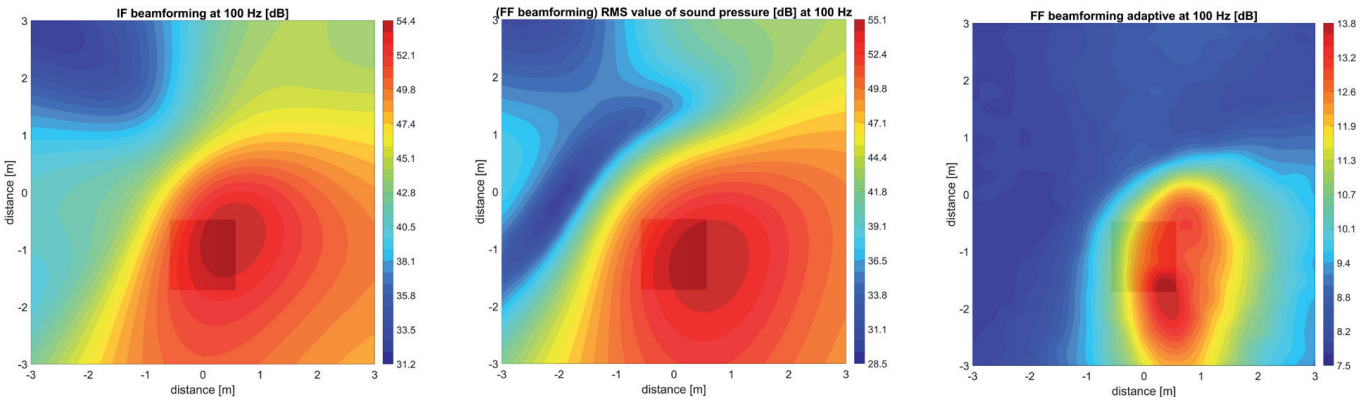

Fig. 7. Localization of regulating transformer noise at a distance of 2 m from the source at 100 Hz frequency using a) conventional infinite focus beamforming, b) finite focus beamforming, c) finite focus adaptive beamforming

Karlo Petrović, Antonio Petošić, Tomislav Župan, Application of Adaptive Finite Focus Beamforming Method for Localization of Low-frequency Transformer Sound, Journal of Energy, vol. 72 Number 4 (2023), 8–14
https://doi.org/10.37798/2023724507

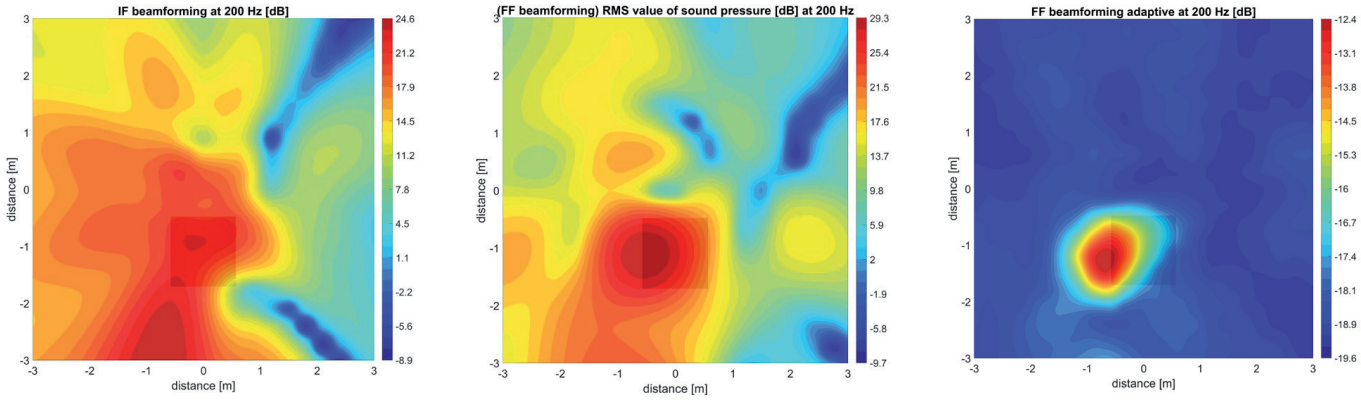

a) b) c)

Fig. 8. Localization of regulating transformer noise at a distance of 2 m from the source at 200 Hz frequency using a) conventional infinite focus beamforming, b) finite focus beamforming, c) finite focus adaptive beamforming

and sound pressure signals are aligned accordingly. The localization of regulating transformer total noise for three beamforming algorithms at a distance from 2 m is shown in Figure 6. The primary noise source is localized at the right side of the regulating transformer using IF beamforming and FF beamforming. As the simulation results from Figure 3 show, the FF beamforming algorithm results in higher accuracy. FF adaptive algorithm localized sound dominantly at the upper right corner and at the regulating transformer's left side. Resolution is increased compared to non-adaptive algorithms.

The localization of regulating transformer noise for three beamforming algorithms at significant transformer noise harmonics (100 Hz, 200 Hz, etc.) is also conducted. Figure 7 shows the localization at 100 Hz component at 2 m from the source. Using FF algorithms (conventional and adaptive), the sound source is localized at the bottom right side of the regulating transformer, and by using the IF algorithm, the sound is localized at the upper right side.The localization of regulating transformer noise at a distance from 2 m at a frequency component of 200 Hz is shown in Figure 8. The sound source is localized at the left side of the regulating transformer using FF algorithms (conventional and adaptive). Localization of the sound source for IF beamforming is more in the middle and at the bottom of the regulating transformerThe localization of re-

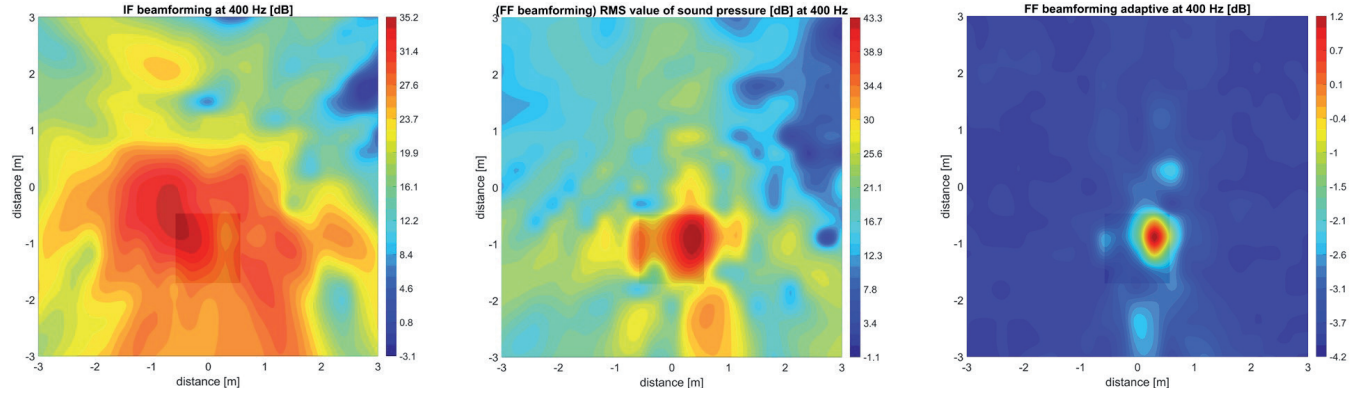

a) b) c)

Fig. 9. Localization of regulating transformer noise at a distance of 2 m from the source at 400 Hz frequency using a) conventional infinite focus beamforming, b) finite focus beamforming, c) finite focus adaptive beamforming

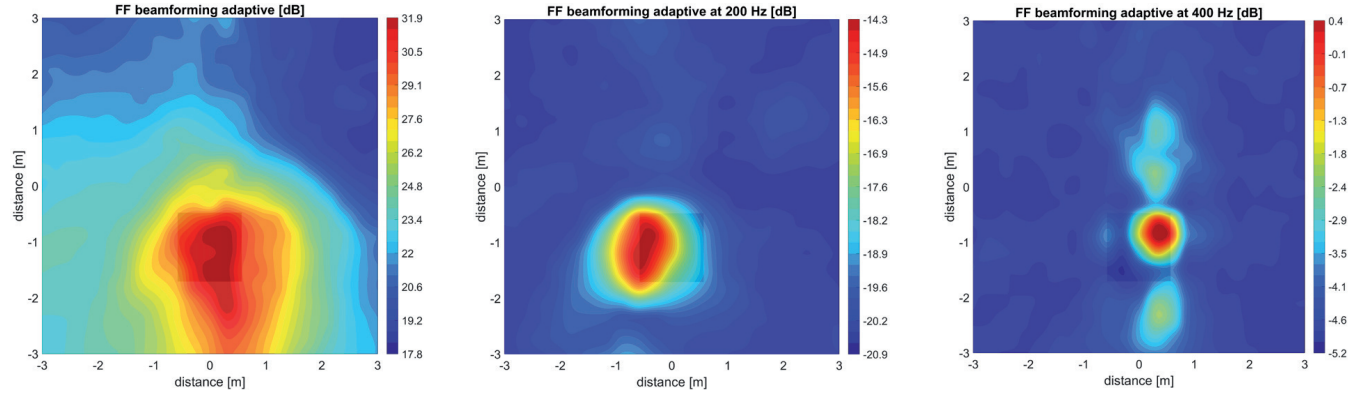

a) b) c)

Fig. 10. Finite focus adaptive beamforming at a distance of 2.5 meters from the source for localization of regulating transformer a) total noise b) noise at 200 Hz frequency c) noise at 400 Hz frequency

Karlo Petrović, Antonio Petošić, Tomislav Župan, Application of Adaptive Finite Focus Beamforming Method for Localization of Low-frequency Transformer Sound, Journal of Energy, vol. 72 Number 4 (2023), 8–14
https://doi.org/10.37798/2023724507

gulating transformer noise at a distance from 2 m at a frequency component of 400 Hz is shown in Figure 9. The sound source is localized at the upper right side of the regulating transformer using FF algorithms (conventional and adaptive). Localization of the sound source for IF beamforming is at the upper left side of the regulating transformer.

The highest resolution is obtained using the FF adaptive beamforming algorithm. Results from measurements at 2 m are compared with measurements at 2.5 m. Total noise from Figure 6c, 200 Hz frequency from Figure 8c, and 400 Hz from Figure 9c are compared with localizations from Figure 10.

A comparison of total noise at two distances shows that adaptive beamforming algorithms are unsuitable for total noise signals. On the contrary, applying the developed method (FF adaptive beamforming) to the filtered single-frequency components (noise harmonics) increased the spatial resolution. Thus, the filtering in combination with an adaptive algorithm in the developed method increases the resolution. Also, the sound source is more accurately localized compared to the conventional infinite focus beamforming.

V. Conclusion

In this paper, three different beamforming algorithms are tested on simulated sources and measurements on the regulating transformer used as a noise source in a semi-anechoic chamber. FF beamforming method with the known distance of the source compared to the conventional IF beamforming method does not increase the resolution. On the other hand, localization accuracy is increased. Except for those two methods, the adaptive FF beamforming method is developed and investigated. This method increases spatial resolution and localization accuracy for low-frequency sounds. A disadvantage of this method is that it is unsuitable for total noise signals. However, transformer noise is at 100 Hz and its harmonics, so it is not a problem to localize specific frequencies at which higher noise levels will occur.

In future work, the automatization of measurements in the form of a robot following the microphone position path can be used. The presented method allows the automatization because a voltage signal aligns pressure signals as if measured at the exact moment. Surface vibration measurement using a laser Doppler vibrometer can also be added to the automatized robot setup to obtain a complete vibroacoustic picture of the transformer, as a continuation of the authors' previous work [11]the vibrations on the surfaces of the tank wall, stiffeners, and the cover of a 5 MVA transformer experimental model were measured during open-circuit and short-circuit transformer tests. Vibration measurements of a transformer tank side were conducted at discrete points using two different voltage sources in no-load test. Using interpolation functions, the RMS values of acceleration and vibration velocity are visualized and compared for each considered measurement configuration (no-load and load tests and two different excitation sources.

Theoretically, even a higher array size can be achieved, which results in increasing spatial resolution. There is only a limit to the space size in which the sound pressure for beamforming is measured. The following step is to test the method in echoic rooms, where applying beamforming and especially adaptive algorithms can be challenging.

References

[1] M. Hrkac, G. Kmita, M. Kozupa, R. Platek, R. Sekula, and R. Zannol, "Vibroacoustic behavior of a small power transformer," in *International Colloquium Transformer Research and Asset Management*, 2012, pp. 1–8.

[2] M. Kucera, R. Jarina, P. Brncal, and M. Gutten, "Visualisation and measurement of acoustic emission from power transformers," *2019 Proceedings of the 12th International Conference on Measurement, MEASUREMENT 2019*, pp. 303–306, May 2019.

[3] M. Gutten, M. Kucera, V. Cefer, P. Brncal, and R. Jarina, "Analysis of Transformers by Acoustic Emission," *2020 IEEE 61st Annual International Scientific Conference on Power and Electrical Engineering of Riga Technical University, RTUCON 2020 - Proceedings*, Nov. 2020.

[4] J. J. Christensen and J. Hald, "Technical Review: No. 1 2004 Beamforming (BV0056)," 2004.

[5] S. Darzi, T. Sieh Kiong, M. Tariqul Islam, M. Ismail, S. Kibria, and B. Salem, "Null steering of adaptive beamforming using linear constraint minimum variance assisted by particle swarm optimization, dynamic mutated artificial immune system, and gravitational search algorithm," *Scientific World Journal*, vol. 2014, 2014.

[6] P. Peng *et al.*, "Design and optimization of noise reduction patch on transformer based on acoustic array technology," *Proceedings 2018 Chinese Automation Congress, CAC 2018*, pp. 1365–1368, Jan. 2019.

[7] M. Sykora and M. Schlosser, "Noise measurement of power transformer," *Proceedings of the International Conference - 2016 Conference on Diagnostics in Electrical Engineering, Diagnostika 2016*, Nov. 2016.

[8] E. Kornatowski, "Vector analysis of transformer tank vibration," *2018 Innovative Materials and Technologies in Electrical Engineering, i-MITEL 2018*, pp. 1–5, May 2018.

[9] D. H. Johnson and D. E. Dudgeon, *Array signal processing : concepts and techniques*. P T R Prentice Hall, 1993.

[10] M. Souden, J. Benesty, and S. Affes, "A study of the LCMV and MVDR noise reduction filters," *IEEE Transactions on Signal Processing*, vol. 58, no. 9, pp. 4925–4935, Sep. 2010.

[11] K. Petrović, A. Petošić, and T. Župan, "Grid-like Vibration Measurements on Power Transformer Tank during Open-Circuit and Short-Circuit Tests," *Energies 2022, Vol. 15, Page 492*, vol. 15, no. 2, p. 492, Jan. 2022.

Journal of Energy

VOLUME 72 Number 4 | 2023

journal homepage: http://journalofenergy.com/

3D Acoustic Heat-Maps for Transformer Monitoring Applications

Ferdinand Fuhrmann, Anna Maly, Martin Blass, Jakub Waikat, Fredi Belavić, Franz Graf

***Summary* — We present a novel approach for measuring and representing acoustic emissions of transformers. The representation of location-based acoustic emissions enables improved monitoring of transformers, e.g., to detect and predict anomalies and failure events. Here, we introduce 3D acoustic heatmaps to visualize the sound emission patterns of a transformer. We use a combined sensing approach consisting of a 3D point cloud, a microphone array, and beamforming algorithms to generate the distributed representation of acoustic emissions over the entire surface of the transformer. In a further step, we intend to apply machine learning methods to the generated data to enable early fault prevention and predictive maintenance.**

***Keywords* — Transformer, Audio, Microphone Array, Monitoring.**

I. Introduction

Transformers are important building blocks of the electrical transmission system. Failure of these components can result in long outages as well as high restoration costs for the grid operator. Therefore, monitoring the condition of transformers and predicting potential failure events are of great interest to all involved parties. A successful monitoring system can thus minimize downtime and prevent transformer failure by triggering tailored predictive maintenance. The most common transformer monitoring techniques include thermal analysis, winding vibration, motion and deformation analysis, dissolve gas analysis, partial discharge analysis, and tapping under load analysis [1].

II. Background

Transformers emit characteristic noise due to the electromagnetic oscillatory behavior of various internal components [2]. These include core and coil oscillations. In addition, partial discharges in the winding insulation and insulating brushes contribute to the noise emissions [3]. Moreover, geomagnetically induced currents and other DC components of the core cause additional noise sources [4]. The combination of the aforementioned factors creates a complex sound field that is further influenced by the age of the transformer, its loading, and potential anomalies [5]. In this paper, a novel approach is developed to use the sound emission patterns of a transformer to represent and monitor the transformer condition during operation. Modelling the acoustic emissions of a transformer enables the detection and prediction of anomalies and failure events. With the here- presented system concept, we introduce additional information for transformer monitoring systems that established methods do not take into account (see Section I).

(Corresponding author: Ferdinand Fuhrmann)

Ferdinand Fuhrmann, Anna Maly, Martin Blass and Franz Graf are with the JOANNEUM RESEARCH Forschungsgesellschaft mbH, Graz, Austria (e-mails: ferdinand.fuhrmann@joanneum.at, anna.maly@joanneum.at, martin.blass@joanneum.at, franz.graf@joanneum.at)

Jakub Waikat is with the Siemens Energy GmbH, Vienna, Austria (e-mail: jakub.waikat@siemens-energy.com)

Fredi Belavic is with the Austrian Power Grid AG, Vienna, Austria (e-mail: fredi.belavic@apg.at)

III. System Overview

We present a novel approach to measure and visualize transformer acoustic emissions. We use the term 3D acoustic heatmap because we visualize the distribution of acoustic emissions over the entire surface of a transformer.

A lidar-generated 3D model of the transformer consists of uniformly distributed voxels. A beamformer algorithm calculates the directional sound radiation of each voxel. The values of the directional sound radiation result in a 3D acoustic heatmap for each desired frequency. These acoustic heatmaps show various information about different parameters, including the distributed sound pressure levels as well as the local sound sources at characteristic frequencies. Using this information, we can create powerful visualization, inspection, and prediction models to assess the condition of the transformer.

IV. Wave Propagation Considerations

Spherical Wave versus Planar Wave. The use of a depth camera provides a great opportunity to use the information about the exact distance of the observed transformer voxels as possible sound sources to each microphone. Usually, it is assumed that the aperture size of a microphone array is small compared to the distance to the sound source. In our case, however, it is not. The Direction of Arrival (DOA) error of the assumed plane wave is therefore no longer negligible.

Figure 1 shows the error of the assumed plane wave. The sound travels from sound source to two microphones, separated by distance d, via r_1 and r_2. We choose the first microphone as the reference microphone, so the plane wave is orthogonal to r_1 and φ is the arrival angle. It can be easily seen that $DOA_{Sphere} = r_2 - r_1$, while $DOA_{Planar} = d \cos \varphi$. Considering the cosine rule, the error resulting from the plane wave assumption depends on three parameters, φ, r_1 and d, respectively.

Ferdinand Fuhrmann, Anna Maly, Martin Blass, Jakub Waikat, Fredi Belavić, Franz Graf, 3D Acoustic Heat-Maps for Transformer Monitoring Applications, Journal of Energy, vol. 72 Number 4 (2023), 15–18
https://doi.org/10.37798/2023724508

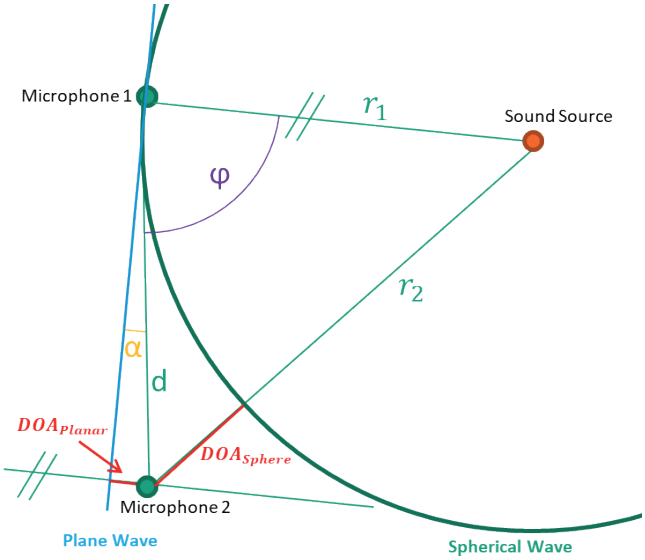

Fig. 1. Error of the plane wave assumption

Figure 2 shows the DOA error at different sound source distances and different microphone distances while keeping the angle of arrival at 80°. Figure 3 shows the DOA error at various sound source distances and arrival angles while the microphone distance is kept at 1 m. The larger the sound source distance, the smaller the error. Moreover, the influence of the error is frequency-dependent; for frequencies with large wavelengths compared to the DOA error, the effect of assuming a plane wave is smaller than for frequencies with small wavelengths, i.e., high frequencies are more affected than low frequencies. A microphone array with an aperture size of about 1 m, a common r1 of 5 m, and an angle of arrival of about 70° has a plane-wave assumption error of around 0.1 m. At 500 Hz, this becomes a wavelength error of about 52°, with 180° representing complete negative interference. The use of a point cloud as possible sound source points gives excellent results for acoustic heat maps and avoids these errors in assuming plane waves.

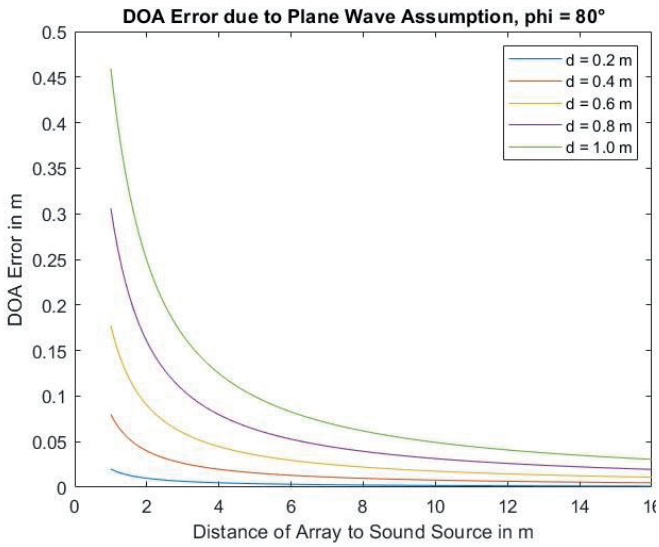

Fig. 2. Error at arrival angle 80°

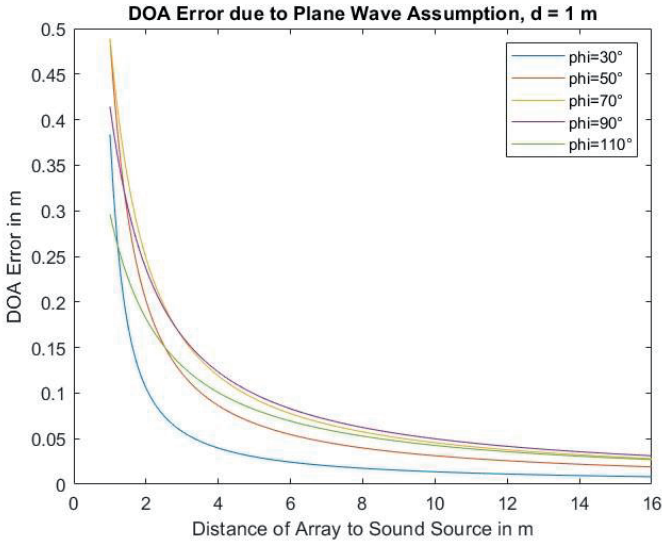

Fig. 3. Error at a microphone interdistance of 1m

V. Implementation

The proposed information processing system consists of a 3D model of the transformer created using a LIDAR scan, a microphone array for audio acquisition, and a beamforming algorithm for processing the multichannel audio data. In the following, we describe the above-mentioned components in detail.

3D Modelling. A 3D model of the transformer created from a LIDAR omnidirectional scan serves as a starting point. Using an RGB-D image taken with a combined visual sensor (RGB and depth), we then register the actual position of the microphone array with respect to the 3D model. In this way, we ensure optimal matching of the different sensor modalities, resulting in the best possible mapping of the audio data to the point cloud.

Microphone Array. The microphone array has a special 3D design that takes into account the desired characteristics in terms of sound distribution as well as mechanical stability and durability.

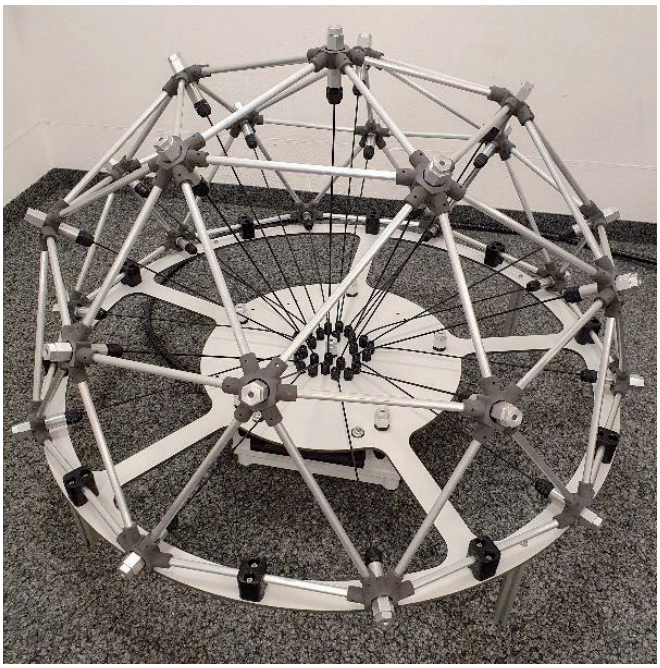

Fig. 4. 32-channel microphone array construction in icosahedron dome geometry.

Ferdinand Fuhrmann, Anna Maly, Martin Blass, Jakub Waikat, Fredi Belavić, Franz Graf, 3D Acoustic Heat-Maps for Transformer Monitoring Applications, Journal of Energy, vol. 72 Number 4 (2023), 15–18
https://doi.org/10.37798/2023724508

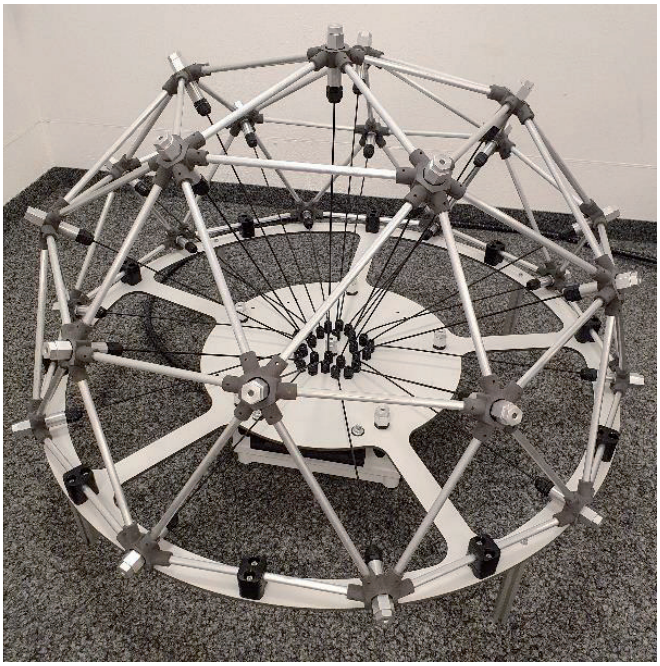

Fig.5. ICP electret microphone inside IP67 enclosure

The geometry consists of an icosahedron dome V2 [6][7] with a radius of 135 cm and 26 vertices mounted on a base plate with 6 holes. This results in 32 sensor positions for ICP electret microphones in an IP67 enclosure. The array geometry was chosen based on numerical beamforming simulations to achieve an appropriate tradeoff between main lobe width and maximum sidelobe levels for third-octave center frequencies within 100 Hz and 20 kHz, resulting in a directivity index greater than 10 dB for frequencies above 200 Hz and greater than 15 dB for frequencies above 800 Hz. The effective spatial aliasing-free frequency range with minimal directionality is 130 Hz to 15 kHz [8]. Fig. 4 and 5 show the array design and the microphone enclosures used for data acquisition.

Beamforming. We use delay-and-sum (DAS) beamforming [9] to compute the sound arriving from a given direction. Beside its straightforward implementation, DAS guarantees artifact-free output signals, which is important for any acoustic modelling approach that relies on these signals. Furthermore, DAS preserves the amplitude ratios with respect to the input signals, which is mandatory for the calculation of the resulting absolute sound pressure values. The use of the 3D point cloud outperforms the typically assumed plane wave, especially for short distances between the microphone array and the transformer. The voxels on the transformer surface serve as sound source positions for the beamforming algorithm. Therefore, the correct spacing of the 3D point cloud significantly improves the radiation pattern.

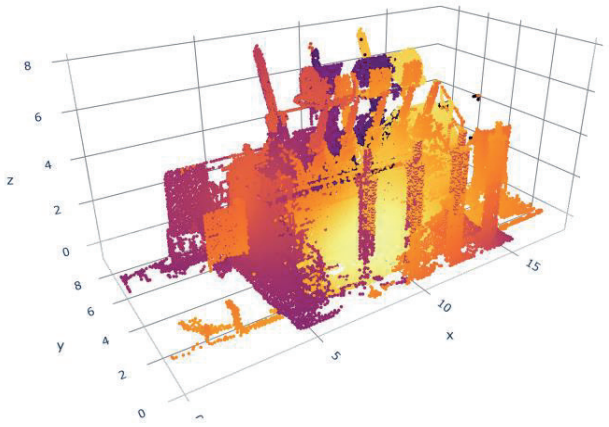

Fig. 6. 3D Heatmap representing the transfomer sound emmissions.

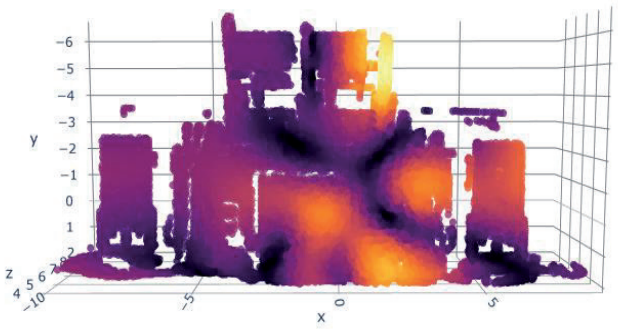

Fig. 7. Broadside heatmap of the transformer for 600Hz.

Fig. 8: Microphone array mounted on a mobile robot during measurements in a substation.

The obtained sound radiation pattern represents the sound radiation of the transformer at the microphone array position. Although we assume the main sound radiation in the orthogonal directions of the transformer, the study of the anisotropic behavior will be a future step. Fig. 6 and 7 show acoustic heatmaps of a transformer for the entire frequency range and a single frequency, respectively. Fig. 8 shows the used microphone array mounted on a mobile robot for data acquisition in a substation.

VI. Results

As a first result, we use the generated 3D acoustic heatmaps to investigate the sound radiation patterns over several characteristic frequencies. In practical applications, we use the system to scan each side of the transformer; the resulting heat maps visualize the all-around radiation patterns at each frequency.

Ferdinand Fuhrmann, Anna Maly, Martin Blass, Jakub Waikat, Fredi Belavić, Franz Graf, 3D Acoustic Heat-Maps for Transformer Monitoring Applications, Journal of Energy, vol. 72 Number 4 (2023), 15–18
https://doi.org/10.37798/2023724508

VII. Conclusions And Outlook

We have presented a novel approach for monitoring the condition of a transformer by creating 3D acoustic heat maps from acoustic sensor data. By combining data from a microphone array with a 3D model of the transformer, we have developed a powerful tool for inspection and modelling. In a next step, we aim to build predictive models by applying machine learning techniques to 3D acoustic heat maps collected during an automated measurement campaign over 3 months [10]. With these models, we aim to automatically predict anomalies as well as potential failure events by analyzing the acoustic radiation patterns emitted by the transformer.

Aknowledgements

This research is funded by the Austrian Research Promotion Agency (FFG) within the project XAMINOR

(881186) and the FFG-COMET-K1 Center "Pro2Future" (Products and Production Systems of the Future), Contract No. 881844.

References

[1] Moravej, Z., and S. Bagheri. "Condition monitoring techniques of power transformers: A review." *Journal of operation and Automation in power Engineering* 3.1 (2015): 71-82.J. Clerk Maxwell, *A Treatise on Electricity and Magnetism,* 3rd ed., vol. 2. Oxford: Clarendon, 1892, pp. 68-73.

[2] Jingzhu, Hu, et al. "Electromagnetic vibration noise analysis of transformer windings and core." *IET Electric Power Applications*10.4 (2016): 251-257.

[3] Bartoletti, Cipriano, et al. "Vibro-acoustic techniques to diagnose power transformers." *IEEE Transactions on Power Delivery* 19.1 (2004): 221- 229.

[4] Bailey, Rachel L., et al. "Modelling geomagnetically induced currents in midlatitude Central Europe using a thin-sheet approach." *Annales Geophysicae*. Vol. 35. No. 3. Göttingen, Germany: Copernicus Publications, 2017.

[5] Tenbohlen, Stefan, et al. "Diagnostic measurements for power transformers." *Energies* 9.5 (2016): 347.

[6] https://en.wikipedia.org/wiki/Icosahedron

[7] https://simplydifferently.org/Geodesic_Dome_Notes?page=3#2V/L2%20Icosahedron%20Dome

[8] Brandstein M., and Ward D. "Microphone Arrays: signal processing techniques and applications." *Springer Science & Business Media* (2001)

[9] Elko, Gary W., and Jens Meyer. "Microphone arrays." *Springer handbook of speech processing* (2008): 1021-1041.

[10] Waikat, J., Jelidi, A., Lic, S., Sopidis, G., Kähler, O., Maly, A., Pestana, J., Fuhrmann, F., Belavic, F. "Preliminary Results by a Multi-Sensor Robot for the Lifecycle Monitoring of Transformers" In Proceedings of the 6th International Colloquium on Transformer Research and Asset Management (ICTRAM), 2023.

Ferdinand Fuhrmann, Anna Maly, Martin Blass, Jakub Waikat, Fredi Belavić, Franz Graf, 3D Acoustic Heat-Maps for Transformer Monitoring Applications, Journal of Energy, vol. 72 Number 4 (2023), 15–18
https://doi.org/10.37798/2023724508

Journal of Energy
VOLUME 72 Number 4 | 2023
journal homepage: http://journalofenergy.com/

Partial Discharge Monitoring of Power Transformers by Calibrated UHF Measurements

Martin Siegel, Christoph Kattmann, Chandra Prakash Beura, Michael Beltle, Stefan Tenbohlen

Summary **— Partial discharge (PD) measurement is an established technique to detect local defects in the oil/paper insulation. They can be measured by electrical PD measurements according to IEC 60270 or by electromagnetic measurements in the ultra-high frequency range (UHF: 300 MHz – 3 GHz). The electromagnetic emissions of PD are recorded using an UHF sensor which is inserted into the transformer tank. The importance of PD measurements is reflected in the standard for charge-based electrical measurements (IEC 60270). Because of the standard, apparent charge, Q_{IEC}, became an essential factor for determining insulation quality in transformers. To be an accepted factor for both, quality testing in factory acceptance tests (FAT) or site acceptance tests (SAT) and continuous PD monitoring, the UHF technology must be as reliable and reproducible as the electrical method. To achieve this, a standardized calibration procedure is needed: It makes UHF measurement results from different systems comparable. Because this calibration procedure was lacking in the past, the UHF technology does not provide comparability between measurement systems and different sensors, yet. However, it shows advantages for on-site acceptance tests like SAT, continuous monitoring, and diagnostic purposes. E.g., regarding signal to noise ratios, the possibility for localization of PD sources and also for practical reasons like preparation times and accessibility on-site. This contribution presents a PD monitoring system which can be calibrated according to the calibration process described recently in Cigré TB 861 and two different types of UHF PD sensors for power transformers. One sensor type is for new transformers using dielectric windows and the other is for retrofitting transformers using their DN50/80 drain valves. A recommendation or strategy on where to place window-type UHF sensors at the tank of new power transformers is also provided in accordance with TB 861. Additionally, this contribution provides a description of the calibration process for UHF PD measurement systems consisting of two steps: 1) Calibration of the measurement instrument analogous to the calibration of the electrical PD measurement circuit using a defined reference signal. 2) Calibration of a UHF sensor using its characteristic antenna factor (AF). Furthermore, it shows three case studies from different power transformers equipped with UHF sensors and UHF PD monitoring systems.**

Keywords **— power transformers, partial discharge, PD, UHF, monitoring, sensors.**

I. Introduction

The reliability of the electrical power grid depends on power transformers. Significant damage and related costs are incurred when a transformer fails. It is important to find any internal damage that is critical as soon as possible. To meet the rising demand for onsite and offsite measurements, various diagnostic techniques have been created [1].

Dissolved gas analysis (DGA) can detect partial discharges indirectly, and electrical PD measurements in accordance with IEC 60270 [2], or by electromagnetic measurements in the ultra-high frequency range (UHF: 300 MHz – 3 GHz)

[3] can detect PD directly. DGA provides a hint for the potential presence of Partial Discharge (PD) in transformers. The use of direct monitoring methods for transformers is increasing. By employing PD measurements, damages to the insulation of power transformers can be quickly identified and subsequently repaired, thereby reducing the risk of transformer failure [4]. Standardized electrical measurement in accordance with IEC 60270, which is required for acceptance at routine testing, highlights its importance. An indication of the quality of a transformer is the conducted apparent charge Q_{IEC}. In terms of monitoring and on-site diagnostics, the electromagnetic UHF method is becoming more significant [5]. The radiated electromagnetic emissions of PD are recorded using an UHF antenna which is installed into the transformer tank. The general differences of the propagation paths of both methods are shown in Figure 1.

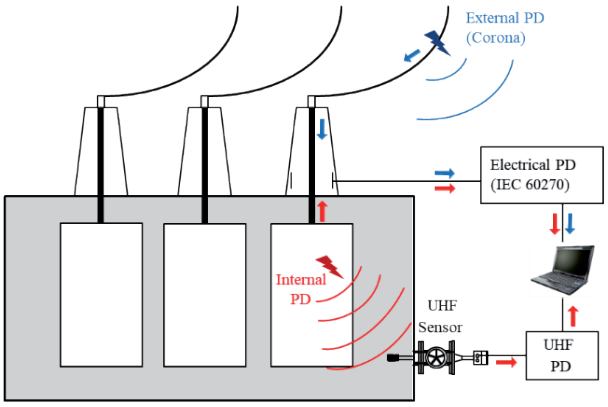

Fig. 1. Signal propagation of UHF and electrical PD measurement at a power transformer with internal PD (red) and external PD (blue) [6]

(Corresponding author: Martin Siegel)
Martin Siegel and Christoph Kattmann are with the BSS Hochspannungstechnik GmbH, Leonberg, Germany (e-mails: martin.siegel@bss-hs.de, christoph.kattmann@bss-hs.de)
Chandra Prakash Beura, Michael Beltle, and Stefan Tenbohlen are with the Institute of Power Transmission and High Voltage Technology (IEH), University of Stuttgart, Stuttgart, Germany (e-mails: chandra.beura@ieh.uni-stuttgart.de, michael.beltle@ieh.uni-stuttgart.de, stefan.tenbohlen@ieh.uni-stuttgart.de)

Martin Siegel, Christoph Kattmann, Chandra Prakash Beura, Michael Beltle, Stefan Tenbohlen, Partial Discharge Monitoring of Power Transformers by Calibrated UHF Measurements, Journal of Energy, vol. 72 Number 4 (2023), 19–27
https://doi.org/10.37798/2023724514

Galvanic coupling allows electrical PD signals to travel through the winding before being decoupled by an external coupling capacitor or by the C_1 capacitance of the bushing for online monitoring. As electromagnetic waves, UHF signals travel through the transformer's oil volume. With the exception of non-graded mid- and low-voltage bushings, the transformer's tank and the low-pass filter of the high-voltage bushings typically protect the UHF PD measurements from outside interference [7]. As a result, when compared to the electrical method, UHF has a tendency to be less susceptible to outside interference. This is advantageous for measurements made in noisy environments, such as those made during continuous PD monitoring and on-site/online PD measurements. As a consequence, Cigré Working Group A2-27 recommends in TB 343 that all transformers should be equipped with DN50 valves for subsequent installation of UHF probes. It also states, that alternatively, dielectric windows can be used for UHF sensors [8]. Both UHF sensor types are discussed in the next chapter. In the subsequent chapter, a recommendation for the placement of window-type UHF sensors at new power transformers is given. Since 2020, a calibration procedure has been introduced [9, 10] which was also incorporated into Cigré TB 861 in 2022 [11]. The method is adopted from established calibration procedures for EMC measurements of radiated emissions defined in CISPR 11 and CISPR 16 [12, 13]. The main target is to ensure reproducibility and comparability of UHF measurements. Both are mandatory for an UHF measurement procedure which can be eventual introduced supplementary to IEC 60270 in the acceptance tests of power transformers.

The primary drawback of the UHF method persists in the demand from many users for a displayed value in picocoulombs (pC) out of convention. Unfortunately, establishing a consistent conversion from radiated UHF measurements to galvanically coupled pC measurements is not universally feasible. In the future, experience must be gained using calibrated UHF measurements to be able to classify the resulting measured UHF PD values, as has been done with the calibrated pC values according to IEC 60270 in the past. One of the main advantages of UHF, the fact that the low-pass filter effect of the capacitive graded high-voltage bushings typically protects UHF PD measurements from outside interference such as corona signals, can also be interpreted as a disadvantage for the detection of PD directly inside the bushings.

II. UHF PD Monitoring System

A comprehensive UHF PD monitoring system for power transformers mainly consist of suitable UHF sensors (described in the following chapter III) and a measurement system which is capable of continuous UHF PD measurement. Such a system should encompass the following features and functionalities:

In many cases, having just a single UHF sensor is inadequate for large power transformers because of their size. To address this, the measurement system should be equipped with multiple analog input channels, enabling simultaneous and ongoing measurement across all these channels. The analog inputs should be capable of the UHF frequency range from approx. 100 – 300 MHz to 2 – 3 GHz with high sensitivity, e.g. -75 dBm, and high dynamic range, e.g. 70 dB. Such a UHF PD measurement system should incorporate data storage and processing capabilities to analyze and interpret PD measurements effectively, e.g., PRPD and trend visualizations. A long-term storage of historical PD data is essential for trend analysis and diagnostics using monitoring data. Also, it should incorporate the option for calibration following the methodology described in Cigré TB 861 [11], as elaborated in chapter IV of this publication.

For the use as a stand-alone PD monitoring solution, the system should feature isolated relay outputs to trigger alerts and actions. A graphical user interface with data visualization tools for real-time and historical PD data analysis is essential for stand-alone monitoring systems, whereas for seamless integration into overlayed monitoring or SCADA systems a UHF PD monitoring measurement system should support industry-standard communication protocols such as ModbusTCP and IEC 61850.

Figure 2a) shows a 2-channel version of a PD monitoring system which can be equipped modularly with up to six analog input channels for electromagnetic (UHF), electrical charge-based (IEC 60270) and acoustic PD measurement. Figure 2b) shows its web interface with a rich visualization of live and historical PD data. It is also compatible not only with power transformers UHF sensors, but also to already installed UHF couplers in GIS for example.

a)

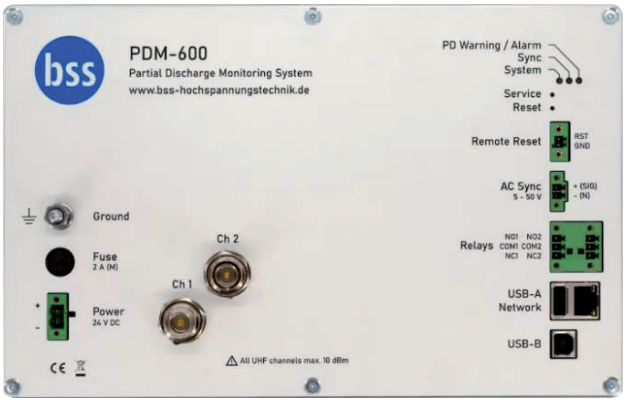

b)

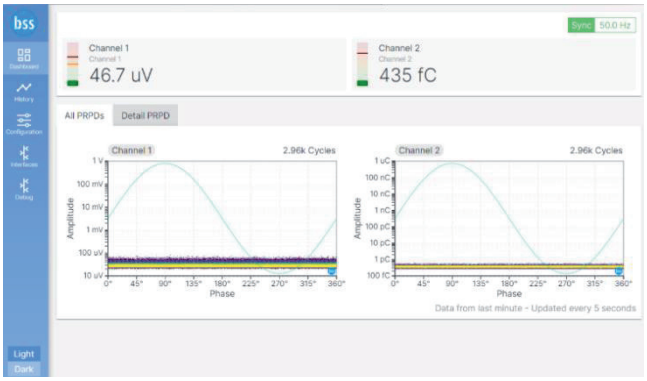

Fig. 2. a) PD monitoring system with 2 UHF channels [14]; b) web-based GUI showing live PD values and PRPDs

III. Types of UHF PD Sensors

A UHF PD sensor consists of a broadband antenna optimized for the UHF frequency range radiated by PD and of its mechanical adaption for installation on power transformers.

A. Drain Valve UHF Sensor

A UHF drain valve sensor (Figure 3a) is designed for transformers, which are equipped with standard DN50 or DN80 gate valves, shown in Figure 3b. Ball and guillotine valves can also be used for sensor installation. To ensure sensor compatibility, it is advised to use straight opening valves on new transformers. The sensors can be installed temporarily on transformers that are in use or being serviced, which is advantageous for on-site diagnostic tests. Permanent installations as a part of an online PD monitoring system are, of course, also possible. To ensure adequate sensitivity, the UHF sensor's head must extend into the transformer's oil space. For most sensor types, an immersion depth of about 50 mm is

Martin Siegel, Christoph Kattmann, Chandra Prakash Beura, Michael Beltle, Stefan Tenbohlen, Partial Discharge Monitoring of Power Transformers by Calibrated UHF Measurements, Journal of Energy, vol. 72 Number 4 (2023), 19–27
https://doi.org/10.37798/2023724514

usually a reasonable value [15]. If the UHF antenna remains in the pipe of the gate valve, the sensor has only a low sensitivity due to the electromagnetic shielding [3].

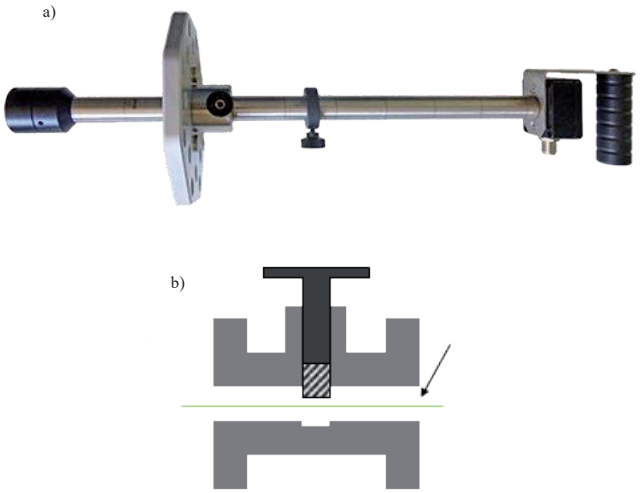

Figure 3 a) UHF drain valve sensor for DN50 / DN80 gate valves [14]; b) Gate valve example for oil valves suited for UHF sensor installation with straight opening [15]

B. Window-Type UHF PD Sensor

For newly constructed transformers or transformers undergoing repairs, window-type UHF sensors, as shown in Figure 4, can be welded directly onto the tank wall. The sensor incorporates a dielectric window. It consists of a stainless-steel welding ring and a high-performance high-temperature and oil-resistant plastic which serves as the oil barrier. Low damping is required for UHF signals to pass through the plastic. The actual sensor is fixed inside the dielectric window (on the air side). Its UHF antenna reaches into the transformer tank inside the dielectric window. Window-type UHF sensors, as opposed to drain valve UHF sensors, can be replaced without handling oil. Cigré Working Group D1-37 recommends a standard design for the welding ring and dielectric window (shown in Figure 4 a) in brochure TB 662 [16] to provide interoperability between sensor manufacturers. Dielectric windows can be located at the transformer tank wall at any suitable location and compatible sensors can then be installed later if needed (UHF PD sensor ready setup).

IV. Calibration of UHF PD Measurements

A standardized calibration procedure in accordance with IEC 60270 ensures the comparability of electrical PD measurement systems and allowed the introduction of acceptance values using the apparent charge Q_{IEC} in the transformer routine tests, although the actual PD charge at the fault location remains unknown.

Both the measurable electrical and UHF PD levels are influenced by:

- Type and magnitude of the PD source
- Position of the PD and the related signal attenuation of the specific coupling path within the transformer tank
- Sensor sensitivity (the UHF sensor, or the coupling capacitor and the quadrupole, respectively)
- Attenuation of measurement cables (more relevant at higher frequencies) and the sensitivity of the particular measurement device.

The coupling path within the transformer cannot be calibrated for either of the PD measurement techniques, leaving neither method's actual PD source level unknown. By removing the influences of sensors and recording devices, calibration can be used to ensure comparability between various measurement devices [11, 17].

Similar to the IEC 60270, a calibration procedure can be used to standardize UHF PD measurement. The UHF calibration procedure, in contrast to electrical PD calibration, entails two steps: calibration of the sensor (by its specific frequency dependent conversion from input electric field to output voltage) and calibration of the combined setup of the entire signal path after the antenna (measurement cable, recording system, amplifier and filters if used).

Therefore, UHF calibration is a two-step process shown in Figure 5. The first step results in the calibration factor K_M and eliminates the influence of the signal recorder and additional accessories, such as additional amplifiers and cable attenuation. This is achieved by using a defined pulse fed into the UHF measurement system at its connection point to the antenna (no UHF sensor is used). This allows any deviations in the measurement to be correc-

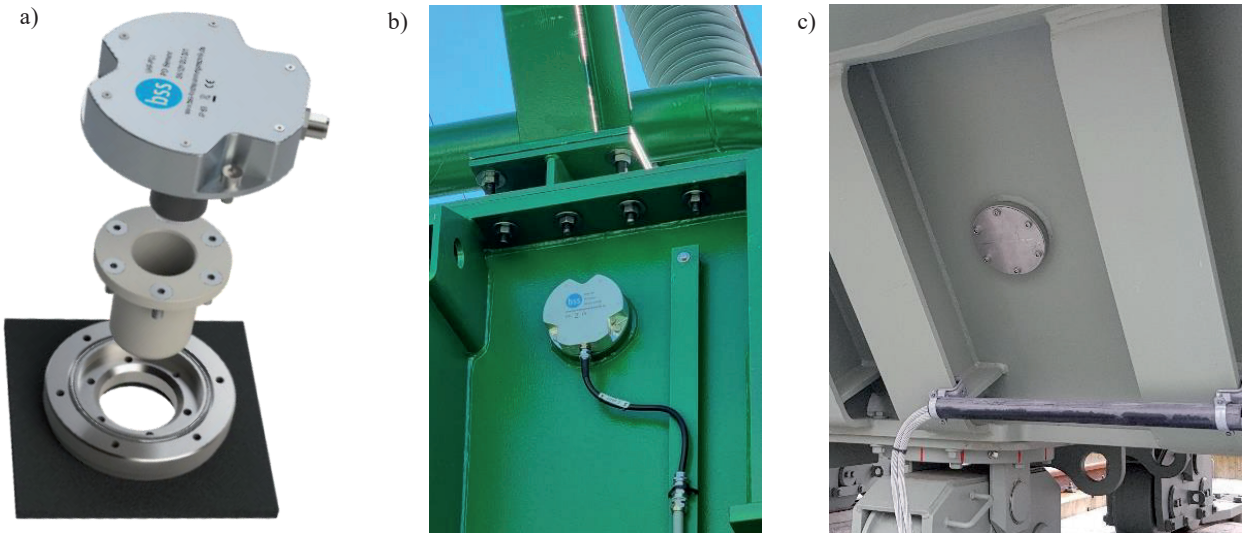

Fig. 4. a) 3D drawing of a welding ring (bottom), dielectric window (middle), and a window-type UHF sensor (top) [14]; b) Installed window-type UHF sensors on a power transformer; c) Dielectric window with blind cover plate (UHF PD sensor ready setup)

Martin Siegel, Christoph Kattmann, Chandra Prakash Beura, Michael Beltle, Stefan Tenbohlen, Partial Discharge Monitoring of Power Transformers by Calibrated UHF Measurements, Journal of Energy, vol. 72 Number 4 (2023), 19–27
https://doi.org/10.37798/2023724514

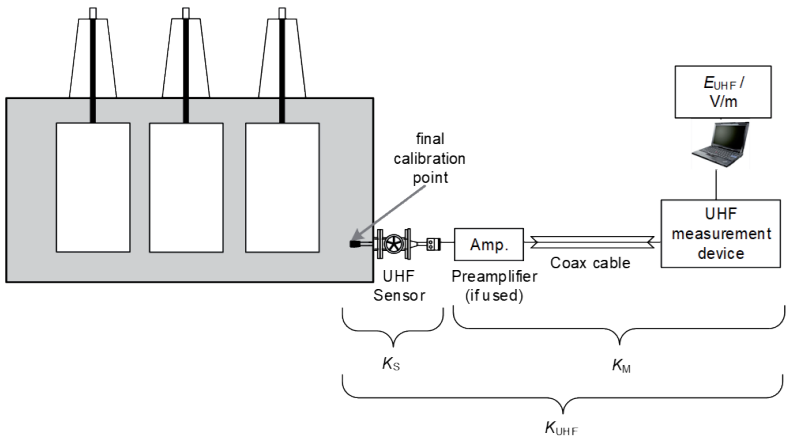

$$K_{UHF} = K_M \cdot K_S \quad [1/m]$$

$$E_{UHF} = K_{UHF} \cdot U_i \quad [V/m]$$

U_i: Indicated amplitude by the UHF instrument
K_M: Measurement device calibration factor
K_S: Sensor calibration factor
K_{UHF}: Resulting calibration factor
E_{UHF}: Measured UHF electrical field strength (after calibration is applied)

Fig. 5. Determination of the calibrated UHF field strength [10]

ted. The second step is performed with the K_S calibration factor. It considers the characteristics of a single sensor, namely its antenna factor (AF), during calibration. The AF represents the ability of a sensor to convert the electric field strength into a voltage signal. It can be measured, for example, with a defined and traceable setup, such as a GTEM cell [18, 19]. These characteristics must be determined by the UHF sensor manufacturer as a precondition so it can then be calculated into the system calibration [9]. The product of both factors with the measured voltage U_i results in the calibrated measured UHF field strength E_{UHF}. which allows comparability between different measurements [9].

V. Sensor Placement Recommendation for UHF PD Monitoring

To be used as a tool for acceptance test, it is necessary that the sensitivity of a PD measuring technique is sufficient to detect ideally all PDs within a power transformer. Based on experimental results obtained from a 300 MVA, 420 kV transformer, a single UHF sensor is unable to provide coverage of the entire tank without the signal becoming noisy [20]. Therefore, at least two sensors are required to provide complete coverage of most tanks. In addition, two sensors are necessary for the performance check procedure (where an impulse is injected into the first sensor and measured by the second to check if both sensors are installed correctly meaning electromagnetically not shielded from the inside of the transformer). Therefore, with respect to factory acceptance tests, two sensors are deemed to be sufficient. However, for UHF based PD source localization, four (shown in Figure 6b) or six sensors are recommended [11].

Results from simulations conducted on a validated power transformer model [21] indicate that if a PD source is located within the windings, electromagnetic waves cannot propagate through the outer layer of windings. Instead, upon encountering the inner surface of the outer winding, the waves are reflected both radially (inward) and axially (along the cooling channels). The axially reflected waves emerge from the top and bottom of the windings and eventually propagate through the oil space in the tank. The simulated propagation characteristics of the waves, which can be observed in Figure 6a, have implications on the sensor positioning: The sensors should be ideally placed above and below the highest and lowest points of the windings, respectively. The different colors show the electromagnetic field (its electric field strength) emitted by a PD in the center of the main insulation gap between HV and LV winding at 12 ns after the PD inception. Simulation results show that above the top height of the winding, detection of EM waves is indeed possible. Thus, the red lines representing the windings bottom / top in Figure 6a represent the installation height thresholds of UHF PD sensors. Experimental results demonstrate that complete tank coverage is achieved by installing one sensor on each lengthwise wall of the transformer tank. [20]. Ideally, the sensors should be positioned at the maximum achievable spatial separation from each other to optimize coverage. Additionally, they should be located in areas with low electric field stress. Experiments conducted on a transformer indicate that UHF sensors

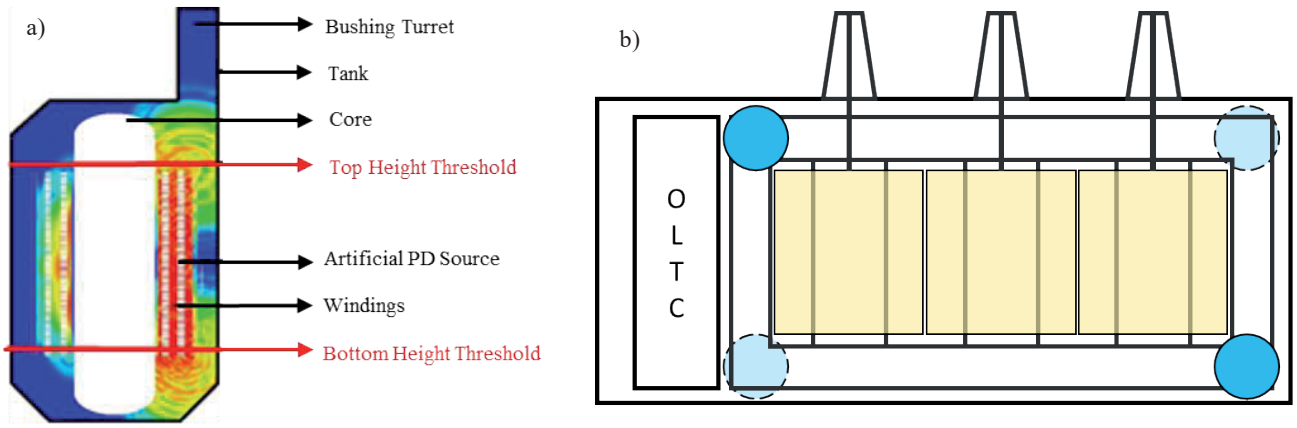

Fig. 6. a) Electromagnetic wave propagation in the tank after 12 ns (sideview) [21]; b) Example for window-type UHF sensor positioning with four sensors [20] complying to the recommendations above.

Martin Siegel, Christoph Kattmann, Chandra Prakash Beura, Michael Beltle, Stefan Tenbohlen, Partial Discharge Monitoring of Power Transformers by Calibrated UHF Measurements, Journal of Energy, vol. 72 Number 4 (2023), 19–27
https://doi.org/10.37798/2023724514

installed on the lengthwise walls of the transformer tank exhibit improved performance when the propagation of electromagnetic waves from the source to the sensor is direct, meaning that minimal obstructions are present. [20]. If the PD occurs near the lead exits, the propagation path can be assumed to be direct. PD inside the windings will inevitably follow an indirect propagation path to reach the sensors (see Figure 6a). Consequently, sensor placement should be determined by signal attenuation concerning both the signal's propagation distance and its propagation path.

An assessment of sensor performance reveals that positions with the least signal attenuation are found near the outer return limbs of the yoke, as indicated by the markings in Figure 6b [22]. Positioned at these locations, sensors exhibit relatively superior performance in comparison to others. Another advantageous aspect of siting a sensor in proximity to the outer return limb is the diminished electric field stress experienced, as the sensor remains further away from the windings, see next paragraph. Hence, it is advisable to place the sensors near the outer limbs of the core forming a diagonal pattern on opposing sides of the tank wall.

For safety reasons, dielectric windows need to be placed in regions with low electric field strength with sufficient distance from the windings and HV lead terminals. Otherwise, for areas with high electrical field strength the air inside the pocket of the dielectric window could lead to PD. It is advisable to follow estimated guidelines regarding the minimum installation distances with respect to the HV winding. For windings rated at 420 kV, 230 kV, and 130 kV, the minimum distances of 1.5 m, 1 m, and 0.8 m, respectively, are recommended [11].

VI. Use Cases

In this chapter, three UHF PD monitoring use cases are presented, each possessing distinct characteristics. One case describes the installation on new power transformers, one describes a retrofit on an old power transformer with known PD issues and one describes the use of UHF PD monitoring after a power transformer fault and repair. The cases occurred prior to the release of CIGRÉ TB 861; as a result, calibration was not conducted on the systems in use. Therefore, the shown PRPD plots show the raw input data of the measurement system (in millivolts).

A. Online Monitoring of Four Identical New Power Transformers

A UHF PD monitoring system was installed at two substations, each equipped with 130 kV power transformers. A total of 12 window-type UHF sensors was installed during the manufacturing of the transformers. Each transformer was connected to a 3-channel PDM-600 PD monitoring system during commissioning, see Figure 7.

In service, PD warnings were triggered on two systems shortly after energization of the transformers. The remote analysis of the PRPDs revealed a stable pattern (see Figure 8, raw input data shown). Other monitoring equipment did not measure any irregularities.

The patterns indicated air bubbles in oil. The source of these gases might be a weakness in the insulation system or an improper filling of the transformer (e.g. non-degassed oil, improper vacuum) and be prone to damages in the future. It was decided to continue normal operation and observe the PD level and patterns for any increase in activity or change in pattern shape. After a few days, the patterns disappeared on both transformers. Accordingly, it was probably not a defect that was outgassing, but trapped air during filling with oil. Since then, monitoring continued and there have been no more abnormalities in the PD data.

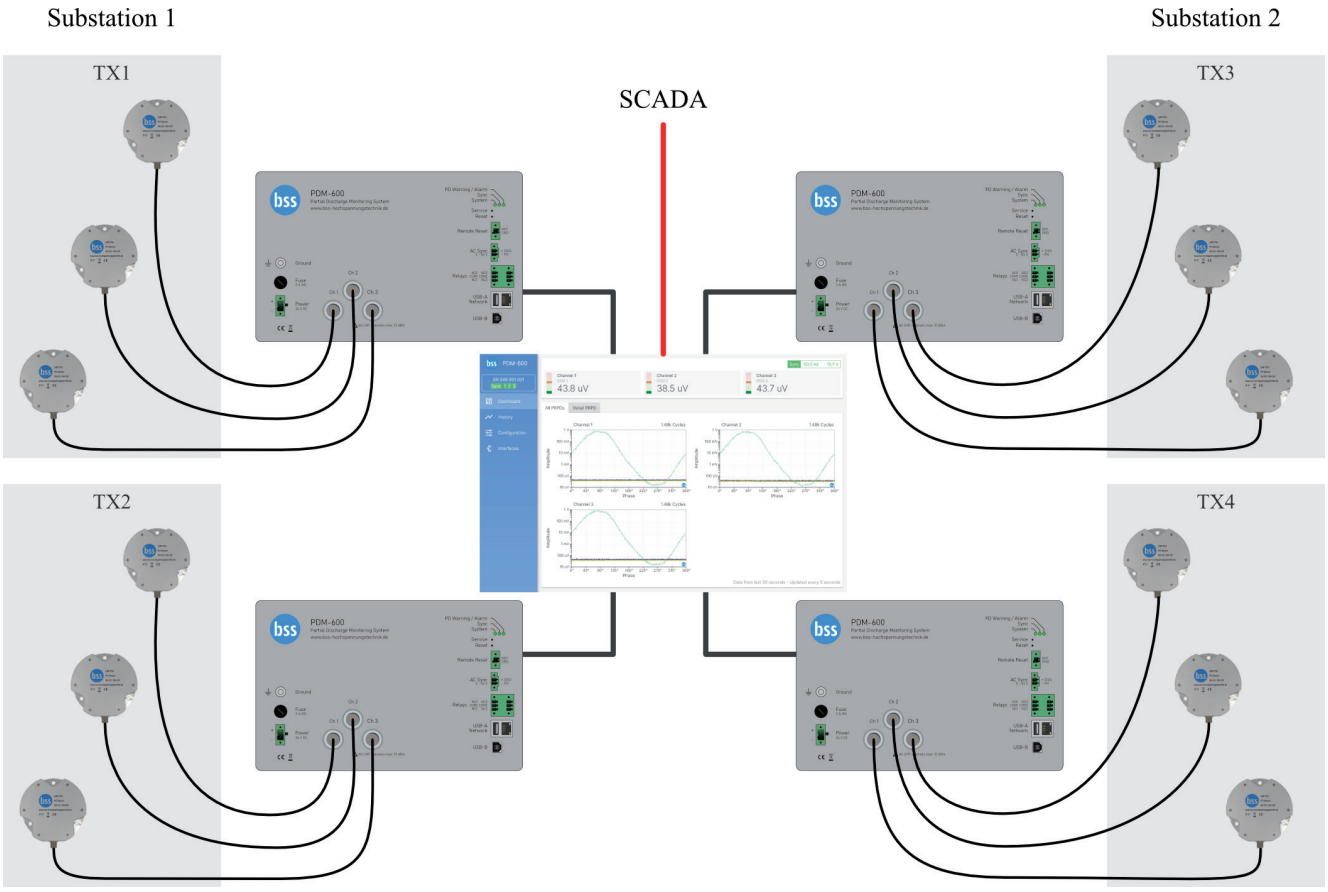

Fig. 7.: Topology of PD monitoring installation with four transformers in two substations

Martin Siegel, Christoph Kattmann, Chandra Prakash Beura, Michael Beltle, Stefan Tenbohlen, Partial Discharge Monitoring of Power Transformers by Calibrated UHF Measurements, Journal of Energy, vol. 72 Number 4 (2023), 19–27
https://doi.org/10.37798/2023724514

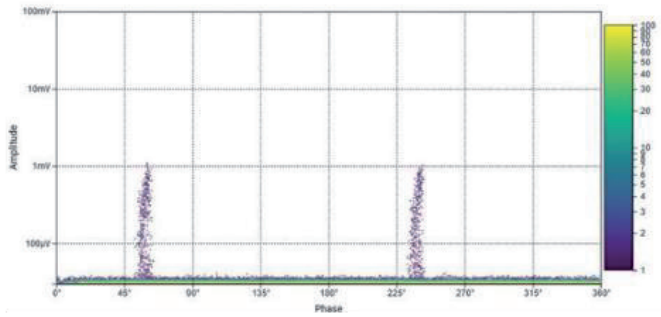

Fig. 8. PRPDs recorded at two of four transformers.

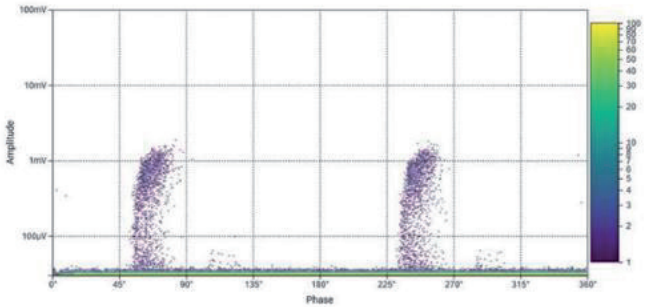

Figure 10 shows the trend view of the PD amplitude correlated to the combined dissolved gas value.

B. Online Monitoring of a 50-year-old 120 MVA, 110 / 10 kV Generator Transformer

This case study presents PD monitoring data of a 50-year-old 110 / 10 kV, 120 MVA generator transformer, which has been monitored for more than six years. Prior to this, the transformer was as a spare unit out of service for eight years. A condition assessment before bringing the unit back into service indicated PD: conventional PD measurements, according to IEC 60270 [2], indicating that the transformer had several active PD sources at nominal voltage U_N with a maximum of 1000 pC.

Due to the lack of standard rules and threshold values to assess old transformers, it was decided that the unit can only be put back into service with continuous PD monitoring. For permanent observation of PD data, a UHF PD monitoring system with a single UHF drain valve sensor was installed (only one gate valve was available). Furthermore, voltages, load currents, top-oil / ambient temperatures, mechanical vibrations, and dissolved gases were recorded. The PD trend was used as an indicator to determine if the insulation defects are worsening. PRPD monitoring data confirmed the presence of more than one PD source. The PDs were not permanently present despite operation of the transformer. Figure 9a shows a UHF PRPD pattern and Figure 9b the same PRPD data time- resolved, whereas the color gradient in Figure 9a represents the number of recorded PD per minute and in Figure 9b the UHF amplitude. The UHF PRPD pattern in Figure 9a shows the PRPD data from Figure 9b from a measurement time set t_1 = 240 min to t_2 = 420 min. High UHF signals occurred in this timeframe which triggered the PD alarm of the system. During this time frame, the amplitude and number of PDs stayed constant and did not get worse, so it was decided to keep the transformer in service, but under close surveillance. After 3 h of high amplitudes, the PD event vanished, and PD activity normalized. The measured combined dissolved fault gases started to increase approx. 4 h after the high amplitude PD event was already over.

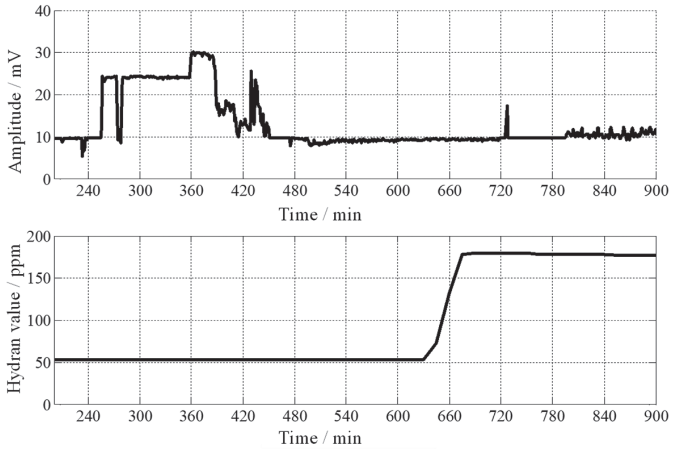

Fig. 10. UHF PD value (top plot) correlated with combined dissolved gas (Hydran) value in ppm (bottom plot)

The alarm threshold for the fault gas value was exceeded approx. 7 h after the high amplitude PD event started. This delay is caused by the gas solubility and dispersion in the transformer. The event illustrates the advantage of direct PD monitoring. The UHF PD monitoring system provides an instant alarm in case of PD events, and PD can be observed using PRPDs and trend views. In contrast, the DGA monitoring alarm occurs with several hours delay (in this case) and no detailed information about the causing PD itself.

C. Online Monitoring of Repaired 40 MVA, 123 kV Substation Transformer

After internal flashover, the active part of a 15-year-old 123 kV substation transformer was cleaned from deposits and carbon particles. After repair, an induced voltage test with partial discharge measurement (IVPD) according to IEC 60076-3 was performed

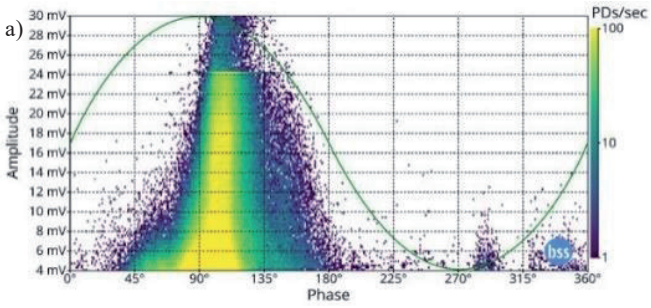

Fig 9. a) UHF PRPD (section 240 min – 420 min in b);

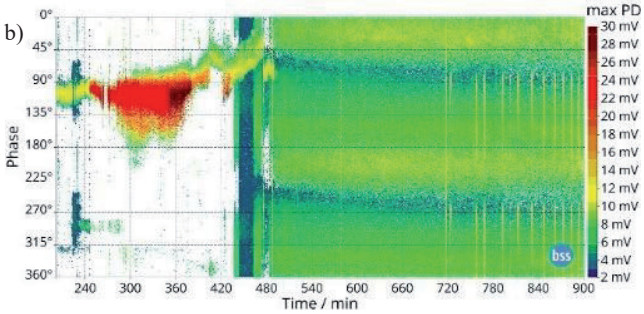

b) time-resolved PRPD (2-dimensional simplification, no #PDs shown)

Martin Siegel, Christoph Kattmann, Chandra Prakash Beura, Michael Beltle, Stefan Tenbohlen, Partial Discharge Monitoring of Power Transformers by Calibrated UHF Measurements, Journal of Energy, vol. 72 Number 4 (2023), 19–27
https://doi.org/10.37798/2023724514

with 80% of the original test level. The test voltage was provided by an inverter. During service, the switching operation of the thyristors produced an interference level of more than 3 nC for the IEC 60270 charge-based PD measurement, which increased to approx. 7.8 nC with increased voltage. Figure 11 shows the charge-based PRPD with thyristor driven disturbances igniting six times within one period. The detection and evaluation of PD with the IEC 60270 based PD measurement system was therefore not possible.

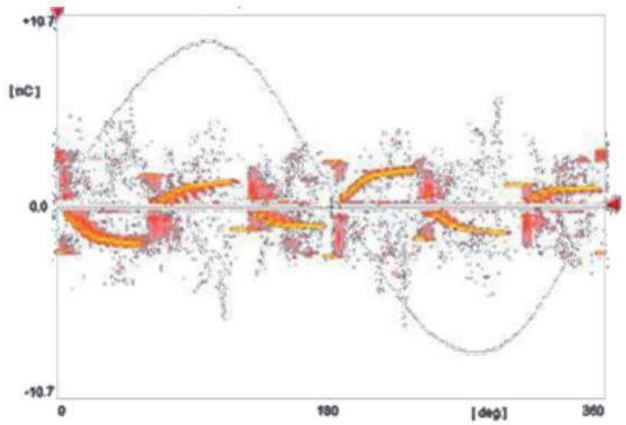

Fig 11. charge-based PRPD according to IEC 60270 with inverter-fed disturbances during factory induced voltage test.

Therefore, the induced voltage test was repeated by using the UHF PD measurement technique which was not affected by the inverter sources. UHF measurements showed significant internal PD (see Figure 12a and Figure 12b). Due to this critical test result, the transformer was equipped with an online PD monitoring system to assess the insulation condition on a permanent basis. Regular oil samplings with particle counting were also carried out.

For UHF PD monitoring, two UHF drain valve sensors were installed on two DN80 oil gate valves. Sensor 1 was mounted on the oil drain valve at the bottom of the tank, while sensor 2 was mounted on the oil valve on top of the tank. Both antennas were installed with an insertion depth of 50 mm to ensure adequate sensitivity.

The online PD monitoring system detected PD activity by both UHF sensors (see Figure 13). The amplitude of the top UHF sensor was higher, see Figure 13b.

Figure 14 illustrates a significant dependence of PD amplitude on oil temperature. This dependence is evident in both short-term and long-term trends. It may result from the temperature-dependent floating behavior of carbon particles that remained within the active part, despite cleaning efforts.

The sustained decline in PD activity over the long term was further validated by DGA samples, as depicted in Figure 15. Nonetheless, owing to the considerably reduced time resolution of DGA analyses when compared to UHF PD monitoring, operational factors such as oil temperature or loading cannot be observed. This use case illustrates how continuous UHF PD monitoring can ensure the secure operation of a network, even in the presence of a problematic transformer.

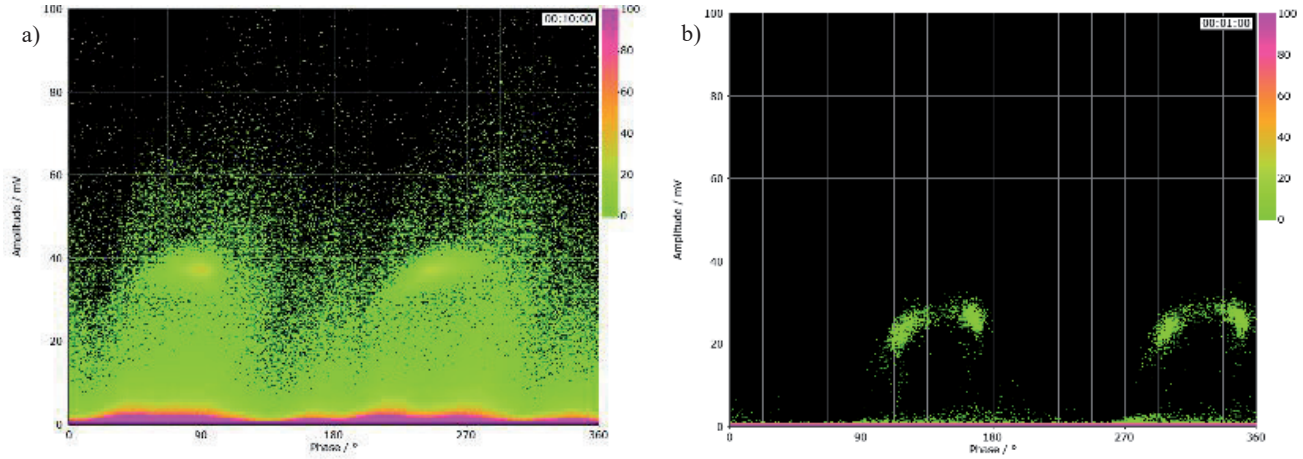

Fig 12. PRPD pattern during factory induced voltage test measured using a UHF drain valve sensor (top); a) at 145 kV; b) at 123 kV

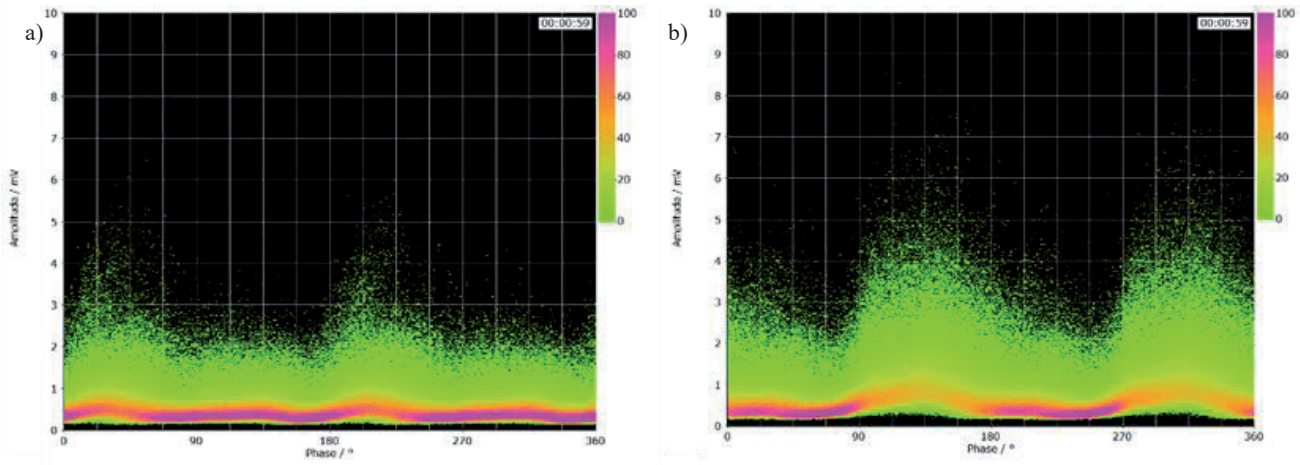

Fig 13. PRPD pattern during operation; a) bottom b) top

Martin Siegel, Christoph Kattmann, Chandra Prakash Beura, Michael Beltle, Stefan Tenbohlen, Partial Discharge Monitoring of Power Transformers by Calibrated UHF Measurements, Journal of Energy, vol. 72 Number 4 (2023), 19–27
https://doi.org/10.37798/2023724514

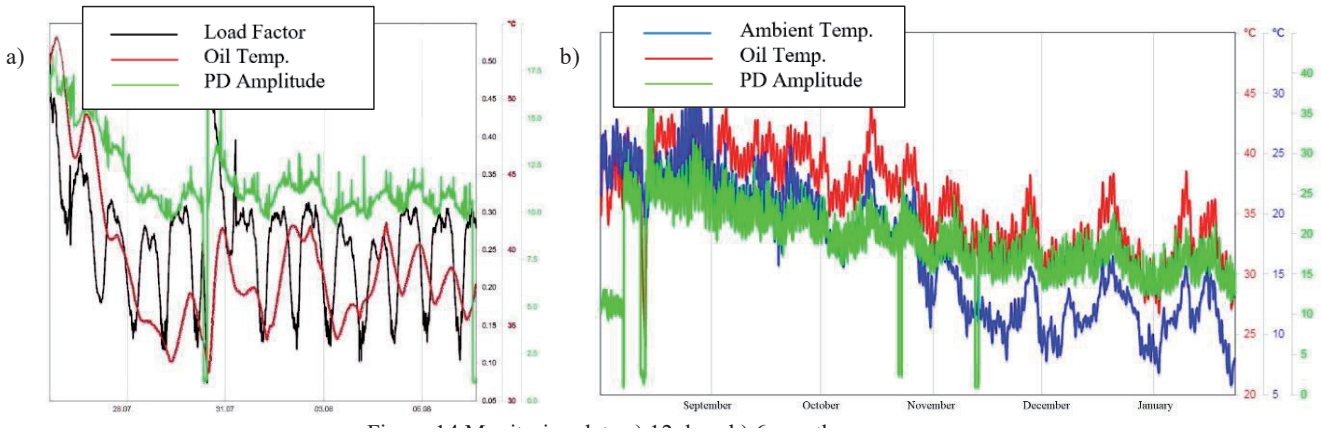

Fig. 14. Monitoring data a) 12 days b) 6 months

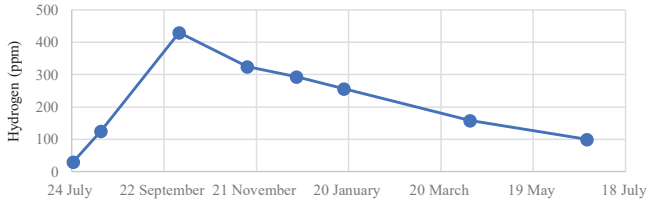

Figure 15 Development of hydrogen content

VII. Conclusions

Power transformers are critical to the reliability of the electrical power grid. Transformer failures result in significant damage and associated costs. All critical internal damage should be detected at an early stage. In addition to the standardized and widely used charge-based PD measurement in factory acceptance tests, it is advisable to consider electromagnetic PD measurement in the UHF range, particularly for assessing power transformers on-site and for continuous online monitoring. As per Cigré TB 861, UHF is recommended for both factory acceptance tests in conjunction with IEC 60270 electrical PD measurements and for permanent on-site PD monitoring. This recommendation stems from its advantages, including high sensitivity and reduced susceptibility to external disturbances.

Out of the two types of UHF PD sensors for power transformers introduced, the drain valve sensors can be installed in transformers equipped with standard DN50 or DN80 gate valves, whereas window-type UHF sensors are installed in dielectric windows provided on the transformer tank wall (meaning usually during construction of a new transformer). The former type is limited by the number and the location of available gate valves but can be used for retrofitting, while the dielectric windows can be placed on the transformer tank wherever desirable on new transformers.

An all-in-one UHF PD monitoring system was introduced, which can be used as a standalone PD monitoring or easily integrated in existing SCADA/monitoring systems using various protocols. It is one of the first UHF PD monitoring system which implemented the UHF calibration procedure recently published in Cigré TB 861. This procedure is needed to obtain two targets: to provide comparability and reproducibility of UHF measurement results from different systems and to incorporate any UHF sensor (with known antenna factor) into individual setups. The UHF calibration process consists of two different steps. The first step provides calibration factor K_M of the entire setup without the antenna The second must be performed by the antenna manufacturer, because the specific antenna characteristics of the UHF sensor (given by the antenna factor).

The positioning of UHF PD sensors on power transformers was discussed. In alignment with the proposal from Cigré TB 861, it is strongly recommended to place at least two sensors to achieve comprehensive and sensitive coverage throughout the entire tank. Additionally, using two sensors allows for performance checks. A reasonable setup consists of four sensors on the tank wall, facilitating UHF-driven localization. UHF installations are cost-effective, as they involve the installation of inexpensive valves or dielectric windows at the factory, with the option to add sensors later, as needed. The optimal sensor positions are near the outer limbs of the core, arranged diagonally on opposing sides of the tank wall, as they offer both sensitivity to UHF signals and a sufficient distance from the high voltage of the active part.

Three case studies of continuous UHF PD monitoring were presented. These studies exemplify the high sensitivity of the UHF method in three distinct scenarios and showcase the minimal noise and interference levels in UHF measurements at transformers in service. In terms of asset management, the examples highlight how PD monitoring can provide additional information to support decision-making processes. For instance, continuous PD monitoring can enable the continued operation of a transformer, even in cases where concerns exist about the equipment.

References

[1] S. Tenbohlen, M. Heindl, M. Jovalekic, A. Müller und M. Siegel, „Trends of the Diagnosis of High Voltage Equipment (Trends in der Diagnostik von Hochspannungs-Betriebsmitteln),“ in *ETG Diagnostik Elektrischer Betriebsmittel*, Fulda, Germany, 2012.

[2] International Electrotechnical Commission (IEC), IEC 60270: High Voltage Test Techniques - Partial Discharge Measurements, Geneva, Switzerland, 2016.

[3] Coenen, S., Measurements of Partial Discharges in Power Transformers using Electromagnetic Signals, PhD Thesis, ISBN 978-3-84821-936-0: Books on Demand GmbH, 2012.

[4] Fuhr, J., „Procedure for Identification and Localization of Dangerous PD Sources in Power Transformers,“ *IEEE Transactions on Dielectrics and Electrical Insulation, Vol. 15, No.5,* 2005.

[5] Judd, M.D., „Power Transformer Monitoring Using UHF Sensors: Installation and Testing,“ in *IEEE International Symposium on Electrical Insulation*, Anaheim, USA, 2000.

[6] S. Tenbohlen, M. Siegel, M. Beltle und M. Reuter, „Suitability of Ultra High Frequency Partial Discharge Measurement for Quality Assurance and Testing of Power Transformers,“ in *CIGRE SC A2 & C4 JOINT COLLOQUIUM*, Zürich, 2013.

Martin Siegel, Christoph Kattmann, Chandra Prakash Beura, Michael Beltle, Stefan Tenbohlen, Partial Discharge Monitoring of Power Transformers by Calibrated UHF Measurements, Journal of Energy, vol. 72 Number 4 (2023), 19–27
https://doi.org/10.37798/2023724514

[7] Judd, M.D., „Partial Discharge Monitoring for Power Transformers Using UHF Sensors Part 2: Field Experience," *IEEE Electrical Insulation Magazine,* Bd. 21, Nr. 3, 2005.

[8] Cigré WG A2.27, Technical Brochure 343: Recommendations for Condition Monitoring and Condition Assessment Facilities for Transformers, Paris, France: Cigré, 2008.

[9] Siegel, M.; Coenen, S.; Beltle, M.; Tenbohlen, S.; Weber, M.; Fehlmann, P.; Hoek, S.M.; Kempf, U.; Schwarz, R.; Linn, T.; Fuhr, J, „Calibration Proposal for UHF Partial Discharge Measurements at Power Transformers.," *MDPI Energies,* 12, 3058 2019.

[10] M. Siegel, Calibration Methods for Reproducible and Comparable UHF PD Measurements in Power Transformers, Stuttgart, Germany: Sierke, 2020.

[11] Cigré JWG A2/D1.51, Technical Brochure 861: Improvements to PD measurements for factory and site acceptance tests of power transformers, Paris, France: Cigré, 2022.

[12] IEC International Special Committee on Radio Interference, CISPR 11: Industrial, scientific and medical equipment – Radio-frequency disturbance, IEC, 2015.

[13] IEC International Special Committee on Radio Interference, CISPR 16: Specification for radio disturbance and immunity measuring apparatus and methods -Part 1-1: Radio disturbance and immunity measuring apparatus – Measuring apparatus, IEC, 2019.

[14] BSS Hochspannungstechnik GmbH, „BSS Hochspannungstechnik," 2023. [Online]. Available: www.bss-hochspannungstechnik.de. [Zugriff am 08 08 2023].

[15] Siegel, M.; Beltle, M.; Tenbohlen, S.; Coenen, S., „Application of UHF Sensors for PD Measurement at Power Transformers," *IEEE Transactions on Dielectrics and Electrical Insulation, Vol. 24, No. 1,* pp. 331-339, 2017.

[16] Cigré WG D1.37, Technical Brochure 662: Guidelines for partial discharge detection using conventional (IEC 60270) and unconventional methods, Paris, France: Cigré, 2016.

[17] Siegel, M.; Tenbohlen, S., „Comparison between Electrical and UHF PD Measurement concerning Calibration and Sensitivity for Power Transformers," in *International Conference on Condition Monitoring and Diagnosis (CMD)*, Jeju, Korea, 2014.

[18] Siegel, M.; Tenbohlen, S., „Design of an Oil-filled GTEM Cell for the Characterization of UHF PD Sensors," in *International Conference on Condition Monitoring and Diagnosis (CMD)*, Jeju, Korea, 2014.

[19] Judd, M.D.; Siegel, M.; Coenen, S., „UHF PD Sensor Characterisation using GTEM Cells," in *ETG Conference*, Berlin, Germany, 2018.

[20] C. P. Beura, M. Beltle und S. Tenbohlen, „Positioning of UHF PD Sensors on Power Transformers based on the Attenuation of UHF Signals," *IEEE Transactions on Power Delivery,* Bd. 34, Nr. 4, pp. 1520-1529, 2019.

[21] Beura, C.P.; Beltle, M.; Tenbohlen, S., „Attenuation of UHF Signals in a 420 kV Power Transformer based on Experiments and Simulation," in *International Symposium on High Voltage Engineering (ISH)*, Budapest, Hungary, 2019.

[22] Beura, C.P.; Beltle, M.; Tenbohlen, S.; Siegel, M., „Quantitative Analysis of the Sensitivity of UHF Sensor Positions on a 420 kV Power Transformer Based on Electromagnetic Simulation".*MDPI Energies 2020, 13, 3.*

[23] R. Lebreton, G. Luna und S. Louise, „Detection and localization of partial discharges in power transformers using four or more UHF sensors," in *International Conference on Condition Monitoring, Diagnosis and Maintenance – CMDM*, Budapest, Hungary, 2013.

[24] Coenen, S.; Hässig, M.; Siegel, M.; Fuhr, J.; Neuhold, S.; Brügger, T.; Hoek, S.M.; Linn, T., „Placement of UHF Sensors on Power Transformers," in *VDE-Hochspannungstechnik*, Berlin, Germany, 2018.

Journal of Energy

VOLUME 72 Number 4 | 2023

journal homepage: http://journalofenergy.com/

Local Aggregator Enhanced Possibilities Coupling Energy Savings and Demand Response Activations

L. Luttenberger Marić, D. Borić, H. Keko, J. Aranda, M. Kirinčić

***Summary* — This paper explores the role of energy communities and local flexibility aggregators in decentralized and decarbonized energy systems. Challenges in the technical and regulatory frameworks of aggregators, with an emphasis on data collection issues, are identified. This work focuses on the essential considerations of coupling long-term energy savings and short-term flexibility activations within a unified program. The paper highlights potential conflicts in optimization goals and emphasizes the necessity for a clear and user-friendly communication between aggregators or energy communities and consumers in order to maintain consumer engagement. The importance of accessible applications for consumer engagement is stressed, with a prioritization of semantic data integration over increased sampling frequency. Sustainable business models are argued for, centred on consistent monitoring of energy savings. Not all consumers are comfortable with in-depth data analysis. The paper suggests the adoption of user-friendly applications for straightforward program monitoring. Emphasis is placed on meaningful data interpretation through semantic integration, rather than a mere increase in data sampling frequency. The argument supports sustainable business models that prioritize consistent monitoring of energy savings and flexibility over reliance on large datasets with limited analytical value. In conclusion, the paper contributes insights into user-centric approaches for sustainable energy communities, emphasizing the integration of long-term energy savings and short-term flexibility within a coherent program.**

***Keywords* — aggregator, demand side flexibility, energy savings, monitoring and verification, data collection**

I. Introduction

The energy system is undergoing continuous changes in the paradigms of energy trading from various heterogeneous sources. At the same time, distributed energy sources (DER) provide diverse aggregation opportunities for the newly emerging energy communities and local flexibility aggregators [1]. By aggregating the granular contributions of individual sources, flexibility aggregators appear as innovative and respectable at system scale flexibility sources at the local level [2]. The amalgamation of various DER, properly selected, categorized, aggregated, and optimized, is opening the path for local flexibility aggregators and energy communities to explore new revenue opportunities on the energy market. Additionally, flexibility aggregators overcome sociological and technological obstacles and activate final consumers in the demand response flexibility programs, where consumers adjust their energy usage based on power grid conditions or price signals.

The limiting factors to unleash their market potential are numerous: challenging assessment of the actual flexibility potential in households due to scarcity or absence of historical data with the desired granularity, overall lack of information of the installed loads in households [3], the inconsistency between quality and quantity of collected data, low level of interoperability between the installed equipment [4], response of consumers to external stimuli, varying socio-economic conditions of consumers [5] and investment possibilities in home equipment, availability of the energy infrastructure (i.e. district heating networks), different building energy performances [6] and climatological conditions, etc. The creation of a sustainable business model for a local flexibility aggregator is a demanding task, especially while considering investment costs which are essential to provide an adequate information and communication framework for data collection, processing, and direct load control for home equipment. In addition, flexibility aggregator should establish a fair compensation for the activation of flexibility of their users (consumers), therefore creating a programme which is adapted to the needs of users, based on their specific characteristics, needs and requirements [7].

The fragmented and very often diverse household market represents both a challenge and an opportunity for the introduction of new business models [8]. The synergetic approach that combines long-term energy savings achieved through energy efficiency measures and short-term energy savings achieved through flexibility activations opens an opportunity for flexibility aggregators to participate in both energy and energy savings markets. In the paper, the principal challenges of participating in both of these markets are assembled and the most indicative approach given the current technical and regulatory situation is discussed.

II. Approach

The paper analyses the requirements for establishing a business model which blends the opportunities for obtaining energy savings on one side and to activate the available demand flexibility and make it available to network operators on the other. The two services are independent and complementary, enabling building residents to enjoy energy savings derived from behavioural

Leila Luttenberger Marić, Donata Borić, and Hrvoje Keko are with the Končar - Digital Ltd., Zagreb, Croatia

(e-mails: leila.luttenberger@koncar.hr; donata.boric@koncar.hr; hrvoje.keko@koncar.hr)

Juan Antonio Aranda Uson is with the Fundacion Circe Centro de Investigacion de Recursos y Consumos Energeticos (CIRCE), Zaragoza, Spain (e-mail: jaaranda@fcirce.es)

Mateo Kirinčić is with the Smart Island Krk Ltd., Krk, Croatia (e-mail: mateo.kirincic@sikrk.hr)

L. Luttenberger Marić, D. Borić, H. Keko, J. Aranda, M. Kirinčić, Local Aggregator Enhanced Possibilities Coupling Energy Savings and Demand Response Activations, Journal of Energy, vol. 72 Number 4 (2023), 28–32
https://doi.org/10.37798/2023724476

change recommendations based on advanced data analytics, and direct remuneration from demand side flexibility aggregated by demand response aggregators and traded in open markets operated by network operators for grid management and balancing. Both services can be delivered simultaneously using the same real-time building data and are not contradictory. Savings come from direct choices made by resident users as a result of behavioural recommendations while aggregated demand flexibility is requested and remunerated by network operators benefiting from short-term flexibility for congestion management and grid balancing. Demand response can be triggered via short term activations delivered by households' consumers, paying specific attention to robust approach in terms of low availability of the data. The introduction of energy efficiency measured in households and the implementation of demand response flexibility programmes are occurrences that could be monitored synergistically for the purpose of achieving common goals in the energy transition. The values of both energy efficiency and demand response directly depend on daily, seasonal, and annual factors which are influencing energy consumption patterns.

A. The Aspects for Establishing a Business Model of A Local Flexibility Aggregator for Residential Consumers

The results of the in-depth analysis for establishing a business model of a local flexibility aggregator for households' consumers are summarized in table 1 and divided in different phases (Phase 0 – Feasibility analysis; Phase 1 – Implementation; Phase 2 – Evaluation and continuous monitoring).

Aspects	*Phase 0 (Feasibility analysis)*	*Phase 1 (Implementation)*	*Phase 2 (Evaluation and continuous monitoring)*
Regulatory framework	Existing regulatory framework enabling the activation of final consumers by flexibility aggregators and market access	Continuous	Continuous
Input data and processing	Data collection and application of proper estimation methods for initial program feasibility assessment	Load profile data and key parameters measurements collection Application of load baseline estimation methods	Continuous evaluation and calibration
Information, communication, and technological framework	Assessment of existing ICT framework and preliminary cost analysis for the installation of new hardware, software and its mutual deployment and calibration Feasibility analysis for setting up a functional standardizes and interoperable framework for data collection and assets control	Establishment and implementation of a functional ICT framework enabling direct load control, with specific accent on scaling and per-user costs	Correct semantic dana interpretation enabling continuous program evaluation and monitoring
Socio-economic	Identification of the main motivational drivers for the consumers involvement and establishing adequate strategies	Application of tailor-made strategies for the program users Continuous customers support	Long-term benefit identification for final consumers
Business and financial	Finding optimal trading modalities for the aggregated flexibility on the energy market markets	Settlement program for the final consumers, trading and	Continuous reprogramming of the flexibility settlement methods

The regulatory framework for establishing relationships among different stakeholders must be taken into consideration in the feasibility assessment, implementation, and evaluation phases. Additionally, clear roles and responsibilities among different stakeholders (aggregator, consumers, and flexibility user i.e., DSO) should be regulated and monitored.

In Phase 0, available flexibility should be assessed based on existing input data, and estimation methods should be developed to evaluate the practicability of a demand response flexibility program on the scrutinized portfolio. The development of proper extrapolation methods is particularly important in cases where there is a consistent gap between data quality and quantity.

In Phase 1, the aggregator should collect energy consumption data as well as data linked to parameters affecting consumption in the desired granularity. Usually, such key parameters affect both users' comfort and energy savings, which is something to consider in monitoring and verification processes for both flexibility calculations and energy savings assessments.

In Phase 2 – the evaluation and continuous monitoring phase, the collection of verified load profiles (usually provided by the DSO) and demand response activation data is imperative. The existence of a technological and communication infrastructure for data collection and storage, as well as the establishment of a standardized architecture for demand response activation, is mandatory in the implementation phase (Phase 1). The ability to monitor information through its semantic interpretation is one of the key features to enable continuous evaluation of flexibility programs (Phase 2).

The correct identification of motivational aspects for triggering customers' interest to participate in demand response flexibility programs should be performed in Phase 0, and appropriate strategies to raise customer awareness should be set up and applied in Phase 1. Moreover, in the implementation phase, such programs require the setting of adequate technical and customer support. Consumers must recognize the long-term benefits of participating in flexibility programs (Phase 2). Finally, for the creation of a financially sustainable business model implementable in the long term, program settlement goals need to be continuously updated and verified (Phases 0 to 2).

While this paper does not explicitly focus on the socio-economic aspects of such programs, it identifies key considerations for their implementation. These include factors such as income levels, cost sensitivity, technological access and literacy, housing conditions, work flexibility, education levels, cultural considerations, and perceived value. The study reveals that, even when analysing a use case with consumers having similar income levels, there can be significant variations in the perceived value among individuals.

B. Load Baselining Approach for Assessing the Engaged Flexibility

In the electricity market environment, transactions are happening continuously between various participants. Consumers can participate in those transactions by offering their flexibility via intermediaries, in exchange of financial compensations [8]. To include a meaningful number of consumers on the electricity market, incentive fees need to be attractive to the consumers and profitable to aggregators. Ultimately, this should result in stable market confidence. Fairness in setting the price is destabilised by the fact that the reduction in consumption cannot be exactly calculated but only estimated. Various load baselining methods simulate the estimated »no event« load, i.e., in absence of a demand response (DR) event [9]. Estimates are primarily based on historical consumption data thus it is necessary to determine

L. Luttenberger Marić, D. Borić, H. Keko, J. Aranda, M. Kirinčić, Local Aggregator Enhanced Possibilities Coupling Energy Savings and Demand Response Activations, Journal of Energy, vol. 72 Number 4 (2023), 28–32
https://doi.org/10.37798/2023724476

the grid user's consumption curve. Ideally, at least one year monitoring of energy consumption data should be considered before entering the electricity market [10]. With their specific consumption curve, grid users are classified into categories that are valued differently. The different categories primarily imply their commercial or non-commercial purpose (whether they are in the private or public sector) and how much flexibility they can offer on the market. The volume of energy necessary to enrol on the market is usually set by the difference between consumer's historic peak load and a demand level that he commits not to exceed during an event. Based on customer's load data it is recommended to determine the weather sensitivity of loads, seasonality (not related to weather conditions) and variability (not related to season or weather conditions) due to different types of methods used in these cases.

Once registered on the market, historical performance can be used to estimate when forecasting the amount of demand response [10]. Based on the theoretical load, the aggregator can calculate the reduction, i.e. difference between the theoretical baseline load and the observed load. This difference is used for assessing payments and penalties for customers. To avoid manipulations by aggregators, load baselining methods should be realistic and transparent to all flexibility providers [9]. Likewise, to avoid manipulations by users, rules and calculation methods should be well defined.

Unlike analytic methods, estimation methods can rarely give exact solution, ergo measurement errors should be included and permitted. However, the error in determining the theoretical baseline increases proportionally in the estimated flexibility engaged as load reduction. In some cases, if load baselining method continuously tends to overstate or understate baseline, it will result in overstated or understated load reduction estimate. Therefore, incentive payments will also be unfairly increased, or reduced.

Load baselining method can be performed in many ways, depending on consumer's category, consumption curve and aggregator's decision. The approach can be summarized in five main steps, visually shown in figure 1.

Baseline window usually includes the last 10 non-holiday weekdays, 10 most recent non-event days, current season or even the whole previous year. Some of these days are not representative or not similar to the day of the event and should be excluded. Exclusion rules usually exclude days with DR events, extreme weather, or days with the lowest or highest loads. Once the data for creating baseline is selected, calculation type of method needs to be specified. Four most used calculation types evaluated on the selected dataset are: average value for each hour of the day, regression, taking the maximum value of the load and rolling average. Created baseline can be further adjusted for conditions of a day-of-event. Most common are additive adjustments which can closely match calculated baseline with measured load. Scalar adjustments are also used but can give more volatile result. To avoid single manipulations, it is recommended that adjustment window relies on a few hours before the time of notification. Other approach is to use weather characteristics for tuning parameters of adjustment method.

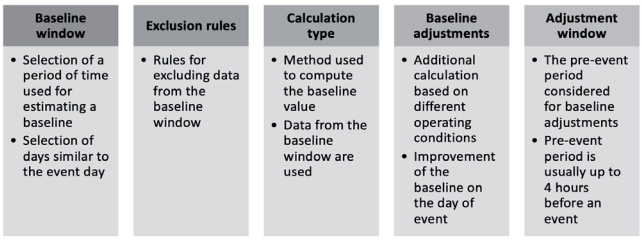

Fig. 1. Five steps for load baselining

C. *Monitoring energy efficiency measures in a dynamic environment*

Monitoring and verification procedures (M&V) are widely used to evaluate the effect of certain energy efficiency measures [11] and the achievement of national energy efficiency goals. The continuous energy transition trends are leading to a progressive digitalization of the energy sector. The integration of automation and management systems in buildings will also provide the means to ESCO companies for better data collection and analysis opportunities of their customer's portfolio [12].

Through an energy performance contracts (EPCs), which is based on achieving client's or consumer's energy savings, an energy service company (ESCO) implements a project to improve energy efficiency or integrate renewable energy sources, by using financial savings obtained from energy savings (as income) to cover investment costs [12]. The ESCOs are responsible for financing and implementing energy efficiency measures and guarantee energy savings. The energy system digitalization and the integration of automation and management systems in buildings should provide the means for better data collection and analysis opportunities of their customer's portfolio.

Monitoring and verification of energy savings and activated flexibility different in approached primarily in terms of data granularity. For any type of user, it is necessary to develop a dedicated load consumption estimate that is directly adapted to user's characteristics, location, typical consumption patterns, etc. Moreover, it is necessary to correctly determine and arrange the main parameters that affect consumption and establish their mutual relations. Figure 2 presents the relation between the typical consumption (with a 15-minute resolution) of two buildings located in the same location and the outdoor temperature. As shown in figure 2 there is no direct correlation between the total consumption of an individual building and the outside temperature, which would mean that regression analysis is not possible.

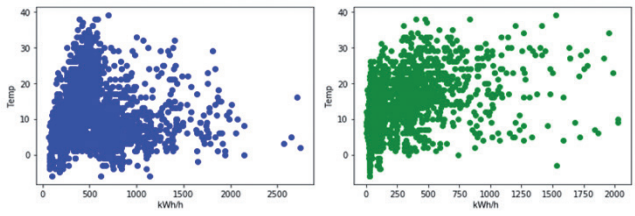

Fig. 2. Outside temperature vs. energy consumption of two different buildings

High data granularity is crucial in the load estimate methods (described in chapter A) necessary for assessing the amount of engaged flexibility, while such approach led to wrong conclusions in determining energy savings.

If a business model considers combined effort opportunities between flexibility and energy savings in a real-time environment, the pay for performance (P4P) models should be considered. Such schemes imply the existence of smart (interval) meters, which register the energy consumption which is therefore normalized and associated with weather conditions [13]. Additionally, with such scheme the uncertainties that a specific measure will lead to savings are minimized, while methods applied for monitoring and verification of energy savings should grant continuous calibration of the calculated savings, therefore minimize errors in assessments.

The monitoring and verification methodology applicable for residential consumers should be based on algorithms that are incorporating both long-term and short-term load reductions that take into account weather and building parameters, seasonal conditio-

L. Luttenberger Marić, D. Borić, H. Keko, J. Aranda, M. Kirinčić, Local Aggregator Enhanced Possibilities Coupling Energy Savings and Demand Response Activations, Journal of Energy, vol. 72 Number 4 (2023), 28–32
https://doi.org/10.37798/2023724476

nal and usual user consumption profiles.

The baseline estimation methods applicable in a P4P scheme could apply regression methods in an environment which is continuously collecting the data. Algorithms should be continuously trained, and load should be estimated, specifically excluding erroneous data and rules should be applied to complete data gaps.

D. Data semantics and parameters to be continously monitored

In the context of data collection, there are several principal aspects to be considered. The "more data is better" principle does not universally apply – it is highly context dependent. The same is valid considering the higher frequency of data sampling. As shown above, the lack of historical higher frequency data is not necessarily the primary obstacle for the proliferation of energy savings and flexibility schemes. Higher granularity (higher sampling frequency) of collected data does increase the baseline estimation and verification precision, but it does so until a certain point of saturation.

This is highly dependent on the context: for instance, implicit short-term flexibility schemes typically need lesser sampling frequency for baselining and verification than the explicit ones. This is entirely expected as implicit ones require behavioural changes and user engagement. However, prematurely restricting the data collection infrastructure could effectively reduce the potential of both energy savings and demand response. Although higher data volume does not always imply higher information content, it is not a good idea to prematurely assume the optimal sampling frequency: too low sampling frequency could leave the end users out of potentially attractive flexibility aggregation schemes. Also, lower frequency data can always be derived from higher sampled ones via resampling.

Moreover, it is not enough to simply gather the data – the collected data must be interpreted correctly and semantically enriched. Though in different households there may be sources of semantically similar data, with no semantic interoperability or with data tied into manufacturer's impenetrable walled gardens, these data are effectively unusable. There have been recent efforts in order to standardize the semantic interoperability across the demand response value chain [14] to remove this problem. The proposed semantic interoperability schemes depart from the existing and established standards (such as SAREF, OpenADR and IEC 61850). In a recent work by the BRIDGE Data Management Working Group [15], a reference architecture for energy data exchange has been proposed, with a layered approach to interoperability. For full semantic interoperability and the data value chain to work, semantic interoperability must function on all technical and semantic layers. For the purposes of monitoring and verifying the effect of a flexibility programme providing energy savings, additional semantic information tied to the data collected from devices and sensors is critical. With no semantic information tied to the data, *ex-post* analysis of the programme's impact may even be misleading.

As increasing the data collection frequency might require significant increases in the cost of data management (e.g. cellular network provider fees in place of using power line carrier communication easily saturated with higher meter readout frequency), when considering the optimal level of data collection, careful analysis should be performed. As indicated here, consistent, and unambiguous interpretation of data is essential and significantly more important than simple increases in data collection frequency.

Moreover, for aggregators installing their own measuring devices for participants could indeed offer several benefits for the aggregator such as:

- Data Accuracy and Control: Aggregators can enhance the accuracy and reliability of the data collected by installing their own measuring devices. This ensures a more precise understanding of participants' energy consumption patterns, allowing for better-informed decision-making.
- Granularity and Detailed Insights: Aggregator-installed devices can provide more granular and detailed insights into participants' energy usage. This granularity is valuable for optimizing demand response strategies, identifying specific areas for improvement, and tailoring programs to individual needs.
- Independence from DSO Schedules: Aggregators, by having their own measuring devices, can access real-time data and respond promptly to changes in participants' energy consumption, maximizing the effectiveness of demand response initiatives.
- Enhanced Program Flexibility: Aggregator-controlled measurements offer greater flexibility in designing and adjusting demand response programs. The ability to capture and analyse data independently allows for quicker adaptation to changing circumstances and ensures a more responsive and agile program.
- Value-Added Services: Aggregators may leverage their own measuring devices to offer additional value-added services, such as energy efficiency recommendations, tailored insights, or even smart home integration. These services can enhance the overall value proposition for participants.

A careful evaluation of the approach is crucial, though: ensuring the accuracy and calibration of the measuring devices, addressing privacy concerns, and coordinating with regulatory requirements are all required. Additionally, open communication with participants about the purpose and benefits of installing such devices can foster trust and transparency. The Implementing Regulation 2023/1162 [16] is especially an implementing act obliging the metering service operators to provide transparent and accessible user access to near real-time metering data. The users are also supposed to be able to delegate the access to their data to third parties authorized by them. This Regulation applies to metering and consumption data, in the form of validated historical metering and consumption data and non-validated near-real time metering and consumption data. As in most EU countries the DSOs are tasked with metering, this regulation effectively obliges the DSO to open the access to the data discussed in this paper. While there may be notable benefits to aggregators installing their own measuring devices, a strategic and well-thought-out approach is crucial to maximize these advantages and ensure a positive impact on the overall effectiveness of demand response programs, especially in light of European policy on the data access to near real time data, acquired by the metering service operators from the official, calibrated and time-synchronized metering devices.

III. Discussion and Conclusions

This article represents a pivotal exploration of a conceptual framework designed to address a significant issue. While the current narrative may give the impression of being centred around existing literature, it functions as the foundational basis for an innovative proof of concept. Moreover, it is imperative to highlight the ongoing efforts within the frESCO project, where similar topics have been rigorously examined. The integration of savings with demand response activations in the framework of the frESCO project has provided valuable insights and practical experiences, establishing a real-world context for the proposed method.

L. Luttenberger Marić, D. Borić, H. Keko, J. Aranda, M. Kirinčić, Local Aggregator Enhanced Possibilities Coupling Energy Savings and Demand Response Activations, Journal of Energy, vol. 72 Number 4 (2023), 28–32
https://doi.org/10.37798/2023724476

The first barrier to overcome in an explicit flexibility programme deployed in residential buildings is the natural rejection of building occupants to grant control of their HVAC equipment to third party companies, thus losing the decision power about their own comfort choices. A human-centric system should be able to forecast users' comfort preferences and assess whether an automated activation may have an effect on the preservation of the users' thermal comfort, either because of a large power shift or a long event duration. In case the comfort boundary conditions are estimated not to be met, the automatic event should not be triggered, and the smart contract rejected prior to the event scheduling. As it stems out of the real tests carried out in the frESCO project demonstration buildings, it is important to avoid user dissatisfaction, or the penalties associated with a failure to deliver the committed flexibility agreed in a market participation smart contract. This is particularly relevant given the fact that short revenues per event are expected considering the low volume of flexibility potential in households.

On the other hand, coupling long-term energy savings and short-term flexibility activations in a same program could lead to conflicted optimization goals. The lack of clarity may result in consumers disorientation and less motivation to enter in such program. This is particularly important within monitoring and verification procedures utilized in transparent ex-post analysis of the program effects. For a user-engaged program to be successful, clarity of its goals as well as consistent and non-ambiguous data interpretation are essential.

It is also not reasonable that an average customer will delve in deep data analysis. Consumers entering the program should be equipped with adequate applications, enabling pragmatic monitoring of current conditions, achieved savings, and activated flexibility. In other words - success of user engagement pay-for-performance program hinges on the palatable presentation of the program benefits. This is valid both in the user engagement and in the operational phase.

For a sustainable business model to be built upon such programs, consistent monitoring of energy savings and activated flexibility is an absolute priority. This is, however, not reachable just by increasing the metering data sampling frequency. Semantic data integration that ensures correct data interpretation across the data value chain is of higher priority than the volume of data. A large-scale dataset that can't be assigned or interpreted has a very low analytic value. Even though higher data granularity certainly increases analysis capabilities, a quite significant part of energy savings benefits can be based upon a quite limited dataset, e.g., monthly or even yearly energy consumption.

Finally, if the short-term flexibility and longer-term energy savings must be opposed, then the implementation of energy savings measures should be prioritized. This means building envelope refurbishment, purchase of energy efficient equipment. Even in medium term horizon, this avoids placing specific focus on the revenue obtained from the market-offered flexibility obtained from short-term activations of engaged loads. In other words, short-term market signals could easily conflict with the total energy savings goals and with generally lower data granularity more significant total effects can be achieved in longer term energy savings domain than in short-term flexibility provisioning.

Acknowledgment

Research leading to these findings has been supported by the frESCO project, which has received funding from the Horizon program under Grant Agreement No. 893857

References

[1] O. Agbonaye, P. Keatley, Y. Huang, O. O. Ademulegun, and N. Hewitt, "Mapping demand flexibility: A spatio-temporal assessment of flexibility needs, opportunities and response potential," *Appl. Energy*, vol. 295, p. 117015, Aug. 2021, doi: 10.1016/j.apenergy.2021.117015.

[2] L. Luttenberger Marić, H. Keko, and M. Delimar, "The Role of Local Aggregator in Delivering Energy Savings to Household Consumers," *Energies*, vol. 15, no. 8, Art. no. 8, Jan. 2022, doi: 10.3390/en15082793.

[3] P. Siano, "Demand response and smart grids—A survey," *Renew. Sustain. Energy Rev.*, vol. 30, pp. 461–478, Feb. 2014, doi: 10.1016/j.rser.2013.10.022.

[4] H. Keko, S. Sučić, L. Luttenberger Marić, P. Hasse, and K. Isakovic, "Widening the Path for Demand-Side Flexibility Services in European Households: Joint findings of the FLEXCoop and HOLISDER projects in standardization and interoperability," 2021. [Online]. Available: https://drive.google.com/file/d/1e4aBUFkA9fIYfVTQwUbQTrVV927VOGtS/view

[5] D. Ribó-Pérez, M. Heleno, and C. Álvarez-Bel, "The flexibility gap: Socioeconomic and geographical factors driving residential flexibility," *Energy Policy*, vol. 153, p. 112282, Jun. 2021, doi: 10.1016/j.enpol.2021.112282.

[6] A. García-Garre, A. Gabaldón, C. Álvarez-Bel, J. L. Martínez-Ramos, L. A. Fernández-Jiménez, and M. Alcázar-Ortega, "Description of a residential Thermal Energy Storage demonstrator: modelling, identification, validation, aggregation and validation of DR performance," in *CIRED 2021 - The 26th International Conference and Exhibition on Electricity Distribution*, Sep. 2021, pp. 1762–1766. doi: 10.1049/icp.2021.1795.

[7] L. Luttenberger Marić, "Modelling of Aggregated Residential Energy Savings Based on Minimal Available Input Data Set," Doctoral thesis, Faculty of Electrical Engineering and Computing, Zagreb, 2022.

[8] C. A. Correa-Florez, A. Michiorri, and G. Kariniotakis, "Optimal Participation of Residential Aggregators in Energy and Local Flexibility Markets," *IEEE Trans. Smart Grid*, vol. 11, no. 2, pp. 1644–1656, Mar. 2020, doi: 10.1109/TSG.2019.2941687.

[9] O. Valentini, N. Andreadou, P. Bertoldi, A. Lucas, I. Saviuc, and E. Kotsakis, "Demand Response Impact Evaluation: A Review of Methods for Estimating the Customer Baseline Load," *Energies*, vol. 15, no. 14, Art. no. 14, Jan. 2022, doi: 10.3390/en15145259.

[10] M. L. Goldberg and C. Goldman, "Measurement and Verification for Demand Response," Electricity Markets and Policy Group, Energy Analysis and Environmental Impacts Division, 2013. [Online]. Available: https://eta-publications.lbl.gov/sites/default/files/napdr-measurement-and-verification.pdf

[11] "Guidelines for Monitoring, Evaluation, Reporting, Verification, and Certification of Energy Efficiency Projects for Climate Change Mitigation | Energy Technology Area." Accessed: Jun. 11, 2022. [Online]. Available: https://energy.lbl.gov/publications/guidelines-monitoring-evaluation-0

[12] L. L. Marić and V. Bukarica, "Combined effort opportunities of aggregated demand response flexibility and energy savings in households," *J. Energy - Energ.*, vol. 70, no. 4, Art. no. 4, 2021, doi: 10.37798/2021704257.

[13] M. Santini, D. Tzani, S. Thomas, V. Stavrakas, J. Rosenow, and A. Celestino, "Experience and Lessons Learned from Pay-for-Performance (P4P) pilots for Energy Efficiency," Zenodo, Jun. 2020. doi: 10.5281/zenodo.3887823.

[14] "Validating SAREF in a Smart Home Environment," springerprofessional.de. Accessed: Mar. 22, 2023. [Online]. Available: https://www.springerprofessional.de/en/validating-saref-in-a-smart-home-environment/18977178

[15] Directorate-General for Energy (European Commission), M. J. Couto, K. Kotsalos, and K. Kukk, *European (energy) data exchange reference architecture 3.0*. LU: Publications Office of the European Union, 2023. Accessed: Oct. 20, 2023. [Online]. Available: https://data.europa.eu/doi/10.2833/815043

[16] "EUR-Lex - 32023R1162 - EN - EUR-Lex - Commission Implementing Regulation (EU) 2023/1162." Accessed: Dec. 29, 2023. [Online]. Available: https://eur-lex.europa.eu/eli/reg_impl/2023/1162/oj

ENERGIJA